HELMHOLTZ
ZENTRUM BERLIN
für Materialien und Energie

Permanent Magnets Including Wigglers and Undulators Part III

Johannes Bahrdt

June 20th-22nd, 2009

Part III

Permanent Magnet Systems

Magnet design considerations
Spectral properties of dipoles and wigglers
Spectral properties of undulators
Undulator shimming for field optimization
Undulator technology
Operation of permanent magnet undulators
Large undulator systems for FELs

Design phase

- function: radiation source, accelerator magnet, industrial application, medical application
  ⇨ tolerance budget for the fields
- magnet stability during assembly and operation
  - baking of in-vacuum undulators (lowest gap)
  - soldering of magnets in a closed circuit (DELTA magnets)
- reproducibility (ppm vs. elect. magn., SC), reliability
- costs related to fabrication and operation (ppm vs. electromagnet)

Construction phase

- FEM-simulations for magnetic and mechanic design
- µm-position accuracy
- compensation of temperature effects
- magnet field measurement, shimming techniques

Peculiarities:

- principally, infinite high fields can be realized though B_r<1.6Tesla
  3.9T ppm dipole: Y. Iwashita, Proc. of PAC (2003) 2198-2200.
- third quadrant operation does not mean low field contribution

Periodic magnet structure with field B and period length λ_0

Constructive interference for the wavelength given by

$$\lambda_n = \frac{\lambda_0}{2n\gamma^2}\left(1 + 0.5 \cdot K^2\right)$$

$$K = 93.4 \cdot B \cdot \lambda_0$$

Halbach I: pure permanent magnet

M=4

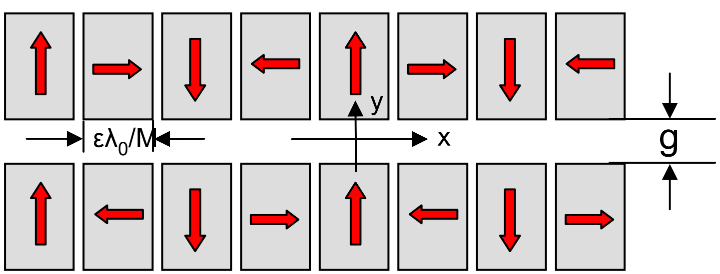

Halbach II: permanent magnet + Fe-pole

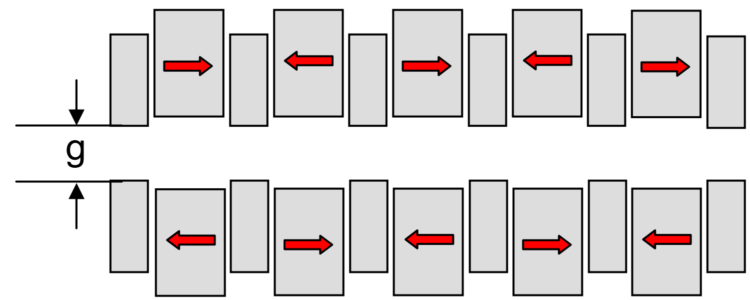

with M=no of magnets / period, ε=filling factor

$$\vec{B}^*(\vec{z}) = i2\vec{B}_r \sum_{\nu=0}^{\infty} \cos(nk\vec{z}) \cdot e^{-nkg/2} \cdot (1 - e^{-nkL}) \cdot \frac{\sin(n\varepsilon\pi / M)}{n\pi / M}$$

$$B_y \approx 3.69 \cdot \exp\left(-5.07 \cdot \frac{g}{\lambda_0} + 1.52 \cdot \left(\frac{g}{\lambda_0}\right)^2\right)$$

$$\vec{z} = x + i \cdot y$$

$$n = 1 + \nu \cdot M$$

$$k = 2\pi / \lambda$$

K. Halbach, Nucl. Instr. and Meth. 187 (1981) 109-117.
"One-sided fluxes -- A magnetic curiosity?"
J. Mallinson, Magnetics, IEEE Transactions on Vol. 9, No. 4 (1973) pp 678 – 682.

Field parametrization:
P. Elleaume et al., Nucl. Instr. and Meth. in Phys. Res. A 455 (2000) 503-523

A Brief History of Insertion Devices

1947	first discussion of undulator radiation by Ginzburg
1951 / 1953	first production of undulator light in the mm and visible regime by Motz et al.
1976	FEL radiation from a superconducting helical undulator at Stanford: Madey et al.
1979 / 1980	first operation of insertion devices in storage rings (SSRL, LURE, VEPP3)
1980...	first operation of wavelength shifters in storage rings (VEPP3, SRS, VEPP2M)
Today	- about 20 third generation synchrotron radiation light sources - SASE FELs operational in the infrared, visible, UV, and X-ray regime (VISA, LEUTL, FLASH, LCLS …)

Classification of Synchrotron Radiation Sources

first generation:

parasitic use of SR at high energy rings,
bending magnets (DESY, DORIS…)

second generation:

dedicated storage rings, bending magnets
and a few insertion devices (BESSY I…)

third generation:

dedicated storage rings optimized for the
use of insertion devices (BESSY II, ALS, ELETTRA, MAX-II…,
SLS, DIAMOND, SOLEIL, ALBA…, ESRF, APS, SPRING-8…)

fourth generation:

linac based SASE-FEL (e.g.: European XFEL, LCLS, SCSS)
seeded FEL such as: cascaded HGHG or EEHG, selfseeding
energy recovery linacs (ERLs)
laser plasma accelerator based table top FEL

The Lienard-Wiechert potentials are the solution of the inhomogenious Maxwell equations

$$\Phi(\vec{x},t)=\left[\frac{e}{(1-\vec{\beta}\cdot\vec{n})R}\right]_{ret}$$

$$\vec{A}(\vec{x},t)=\left[\frac{e\vec{\beta}}{(1-\vec{\beta}\cdot\vec{n})R}\right]_{ret}$$

The brackets are evaluated at the retarded time:

$$t'=t-R(t')/c$$

The acceleration and velocity fields are derived from these potentials:

$$\vec{E}^{acc}(t)=\frac{e}{4\pi\varepsilon_0 c}\cdot\left[\left(\vec{n}\times\left[(\vec{n}-\vec{\beta})\times\dot{\vec{\beta}}\right]\right)\Big/\left(R\cdot(1-\vec{\beta}\cdot\vec{n})^3\right)\right]_{ret}$$

$$\vec{E}^{vel}(t)=\frac{e}{4\pi\varepsilon_0}\cdot\left[(\vec{n}-\vec{\beta})\Big/\left(\gamma^2\cdot R^2\cdot(1-\vec{\beta}\cdot\vec{n})^3\right)\right]_{ret}$$

$$\vec{B}=\frac{1}{c}\left[\vec{n}\times\vec{E}\right]_{ret}$$

Radiation Emitted by Accelerated Charged Particles

$$\frac{\partial^2 I}{\partial t \partial \Omega} = \left|\vec{S}\right|^2 R^2$$

$$\vec{S} = \vec{E} \times \vec{H}$$

The emitted power is given by the poynting vector $\vec{S}$

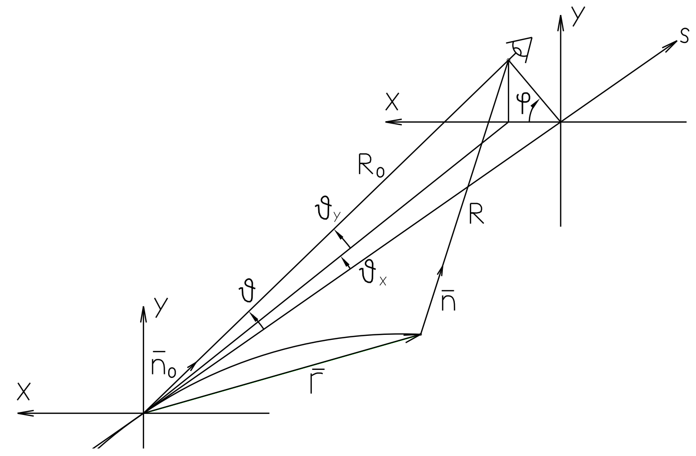

The spectrum is evaluated via a Fourier transformation of the time dependent fields

$$\frac{\partial^2 I}{\partial \omega \partial \Omega} = \frac{e^2}{16\pi^3 \varepsilon_0 c} \left| \int_{-\infty}^{\infty} \left[\left(\vec{n} \times \left((\vec{n} - \vec{\beta}) \times \dot{\vec{\beta}} \right) \right) \Big/ (1 - \vec{\beta} \cdot \vec{n})^3 \right]_{ret} e^{i\omega t} dt \right|^2$$

In the far field we approximate:

$$R(t') \approx R_0(t') - \vec{n}_0 \cdot \vec{r}(t')$$

$$\vec{n} = \vec{n}_0$$

$$\frac{\partial^2 I}{\partial \omega \partial \Omega} = \frac{e^2}{16\pi^3 \varepsilon_0 c} \left| \int_{-\infty}^{\infty} \left[\left(\vec{n} \times \left((\vec{n} - \vec{\beta}) \times \dot{\vec{\beta}} \right) \right) \Big/ (1 - \vec{\beta} \cdot \vec{n})^2 \right] e^{i\omega(t - \vec{n}\cdot\vec{r})} dt \right|^2$$

Bending Magnets, Flux Density, Flux

$$\frac{\partial^2 I}{\partial\omega\partial\Omega} = \frac{3e^2}{16\pi^3\varepsilon_0 c} y^2\gamma^2(1+X^2)^2\left|K_{2/3}(\xi), -i\sqrt{X^2/(1+X^2)}K_{1/3}(\xi)\right|^2$$

$$\xi = \frac{y}{2}(1+(\gamma\theta_y)^2)^{3/2}$$

$$y = \omega/\omega_c$$

$$\omega_c = (3\gamma^3 c)/(2\rho)$$

ρ=bending radius

E_x E_y

The critical energy divides the power spectrum into equal parts.

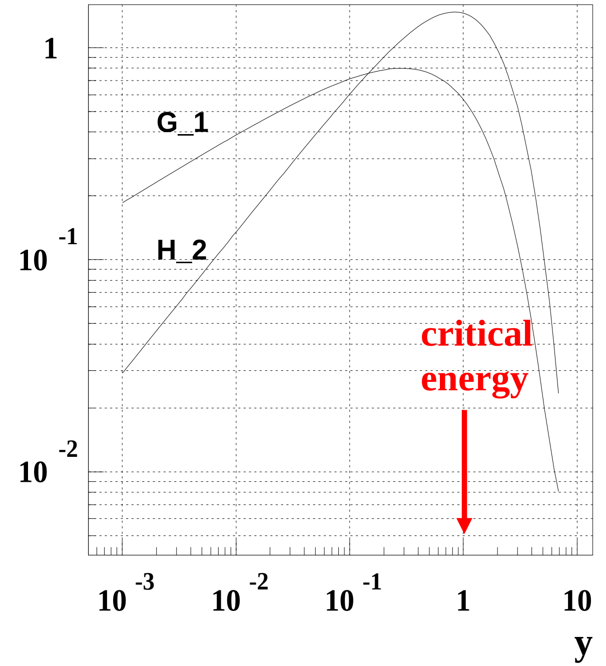

on axis flux density (ph / s / mrad**2 / 0.1%BW)

$$\frac{\partial^2 \tilde{F}}{\partial(\Delta\omega/\omega)\partial\Omega} = 1.327\cdot 10^{13}\cdot E(GeV)^2\cdot I(A)\cdot H_2(y)$$

vertically integrated flux (ph / s / mrad / 0.1%BW)

$$\frac{\partial^2 \tilde{F}}{\partial(\Delta\omega/\omega)\partial\theta_x} = 2.457\cdot 10^{13}\cdot E(GeV)\cdot I(A)\cdot G_1(y)$$

The critical energy scales with the second power of the electron energy

Wiggler: A Sequence of Alternating Dipoles

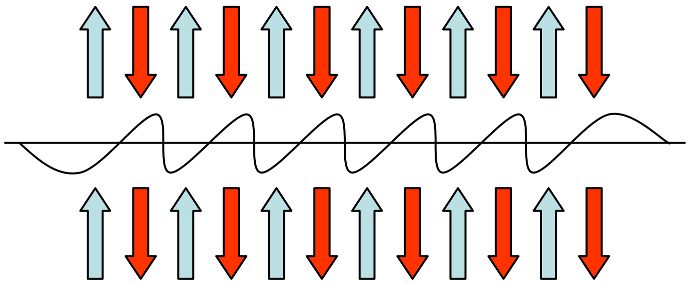

brilliance scales linearly with number of poles
incoherent overlap of light from individual poles
spectrum = n times dipole spectrum

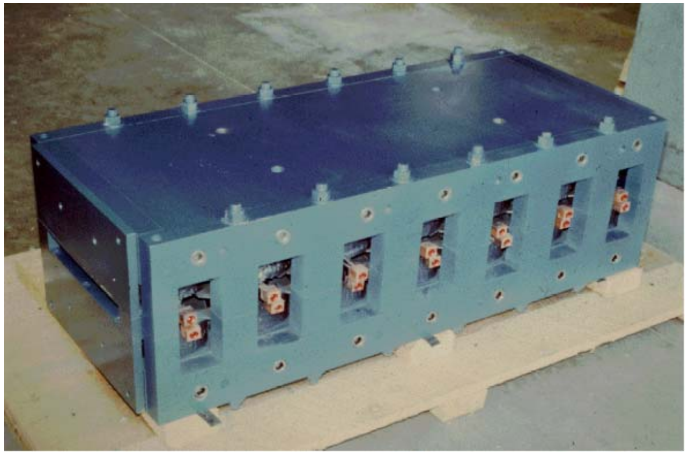

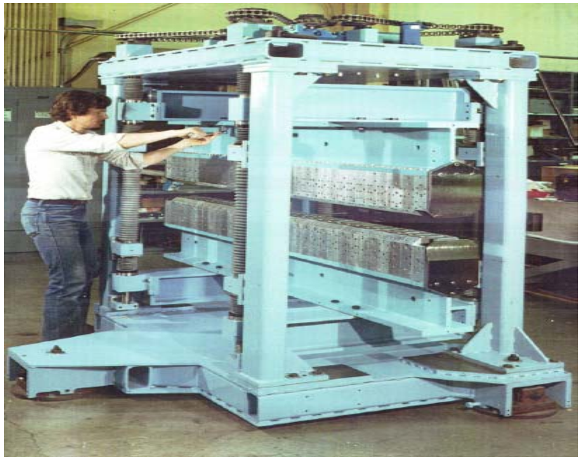

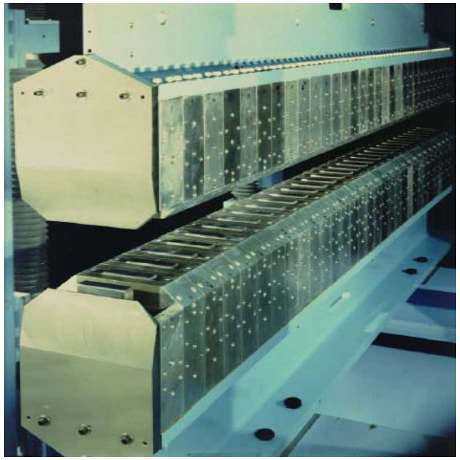

SSRL 1978
Electromagnetic 7 poles wiggler

LBL / SSRL 1985
54 poles hybrid wiggler

Bending Magnets, Polarization

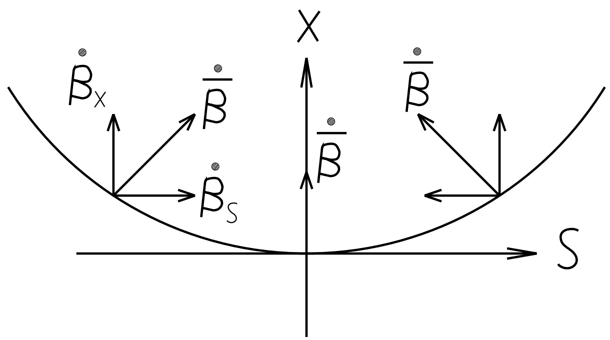

$$\beta_y = \dot{\beta}_y = 0 \qquad \text{(B-field in y-direction)}$$

$$\Delta E_x \propto -\dot{\beta}_x \cdot \left(n_y^2 + n_s^2\right) + \dot{\beta}_s \cdot n_x n_s + \left(-\beta_x \dot{\beta}_s + \beta_s \dot{\beta}_x\right) \cdot n_s$$

$$\Delta E_y \propto \dot{\beta}_x \cdot n_x n_y + \dot{\beta}_s \cdot n_y n_s$$

small
symmetric
antisymmetric

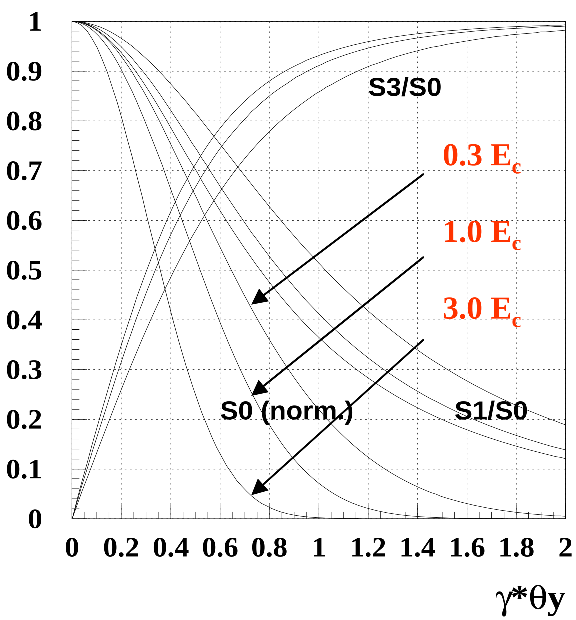

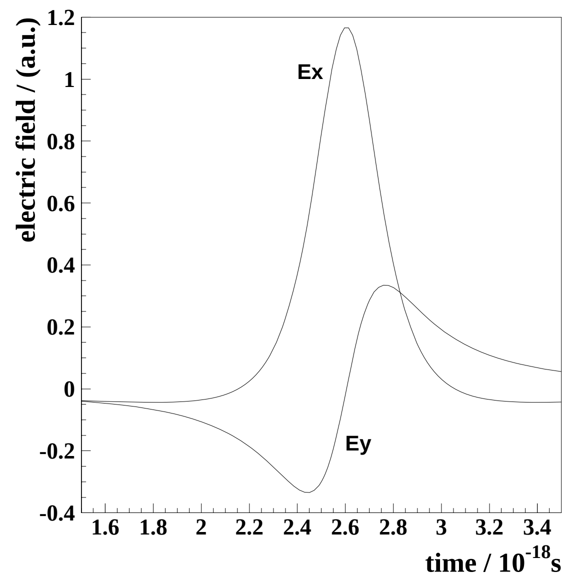

ΔE_x and ΔE_y

are out of phase by: $\pi / 2$

S1/S0=degree of linear poalrization
S3/S0=degree of circular polarization

Circularly polarized off plane bending magnet radiation was widely used at BESSY I

DESY, ESRF

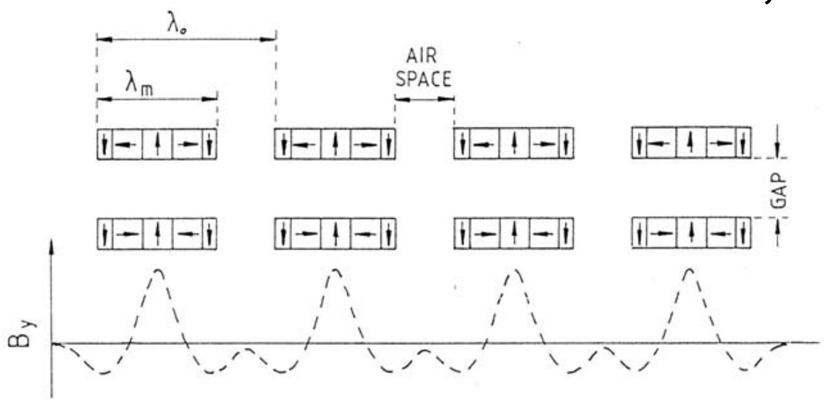

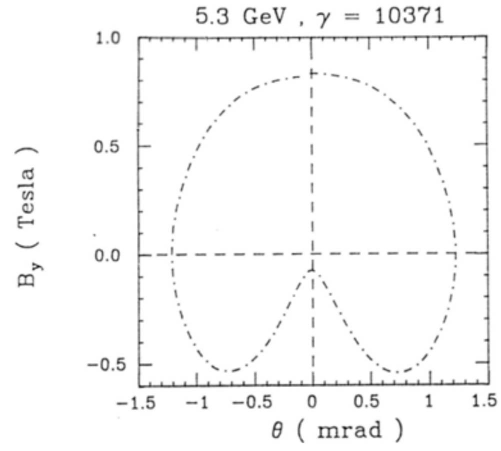

J. Pflüger, G. Heintze, Nucl. Instr. and Meth. 289 (1990) 300-306
J. Goulon et al. Nucl. Instr. and. Meth. 254 (1987) 192-201

Asymmetric wiggler, ESRF
Hybrid type, B = 3.1 Tesla
gap = 11mm, λ = 378mm

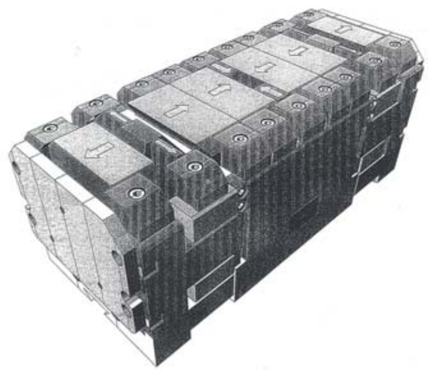

Helicity switching via changing the observation angle

J. Chavanne, P. Van Vaerenbergh and P. Elleaume, Nucl. Instr. And Meth. in Phys. Res. A, 421 (1999) 352-360

Elliptically Polarizing Wigglers: Other Designs

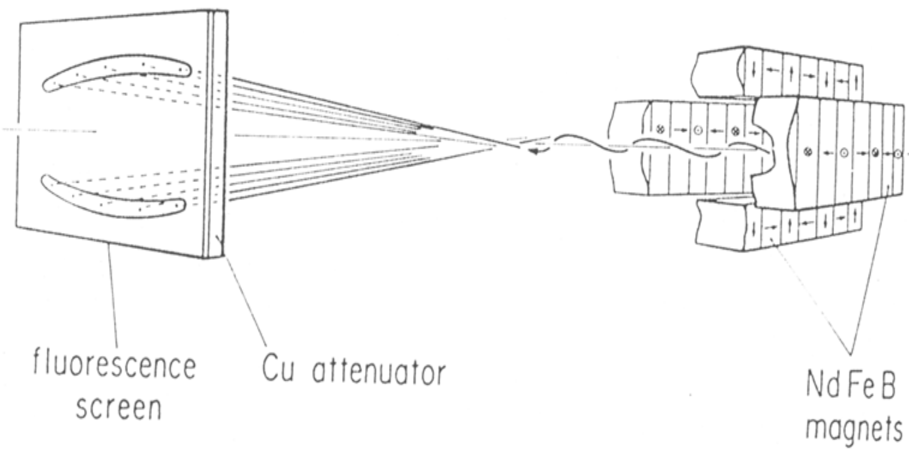

S. Yamamoto et al., Phys. Rev. Lett., 62 (1989) 2672-2675

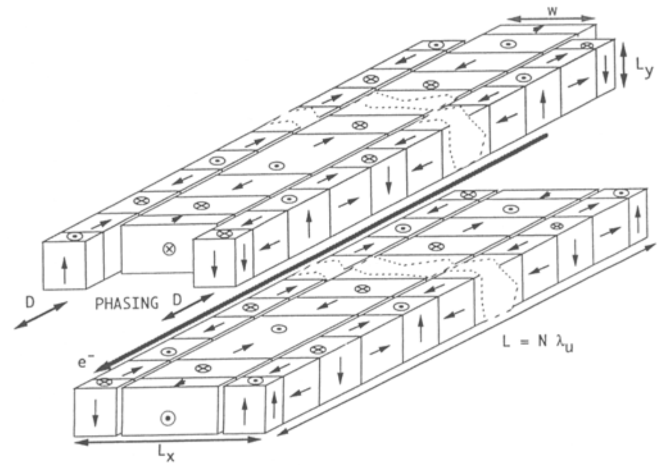

X. M. Marechal et al., Rev. Sci. Instr. 66 (1995) 1937-1939

Helicity Switching via mechanical movement of magnet rows

Undulator Radiation

resonance condition

$$\lambda = \frac{\lambda_0}{2\gamma^2}\left(1 + K^2/2 + \gamma^2\theta^2\right)$$

$$K = 93.4 \cdot \lambda_0 \cdot B_0$$

figure 8 motion in moving frame
produces higher harmonics
on axis: only odd harmonics

$$x(t) = \frac{Kc}{\gamma\omega_u}\sin(\omega_u t)$$

$$s(t) = \bar{\beta}ct - \frac{K^2 c}{8\gamma^2\omega_u}\sin(2\omega_u t)$$

off axis: also even harmonics

electric field at observer   spectrum

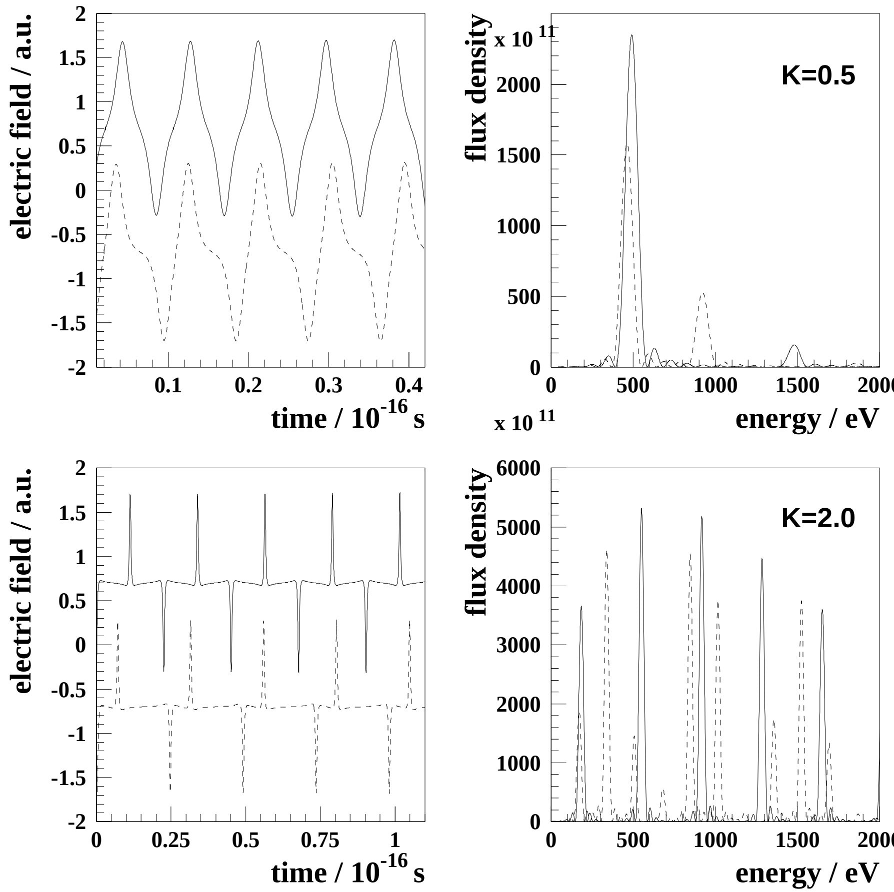

Analytic Approach for Undulator Radiation

$$\frac{\partial^2 I}{\partial\omega\partial\Omega} = \frac{e^2\gamma^2 N^2}{4\pi\varepsilon_0 c} \cdot F_n(K_x, K_y, \gamma\theta, \gamma\Phi) \cdot \frac{\sin^2(N\pi\cdot\Delta\omega/\omega_1(\theta))}{N^2\sin^2(\pi\cdot\Delta\omega/\omega_1(\theta))}$$

Fn represents an infinite sum over BESSEL functions.
The line shape function (last term) describes the interference effects.

Fn

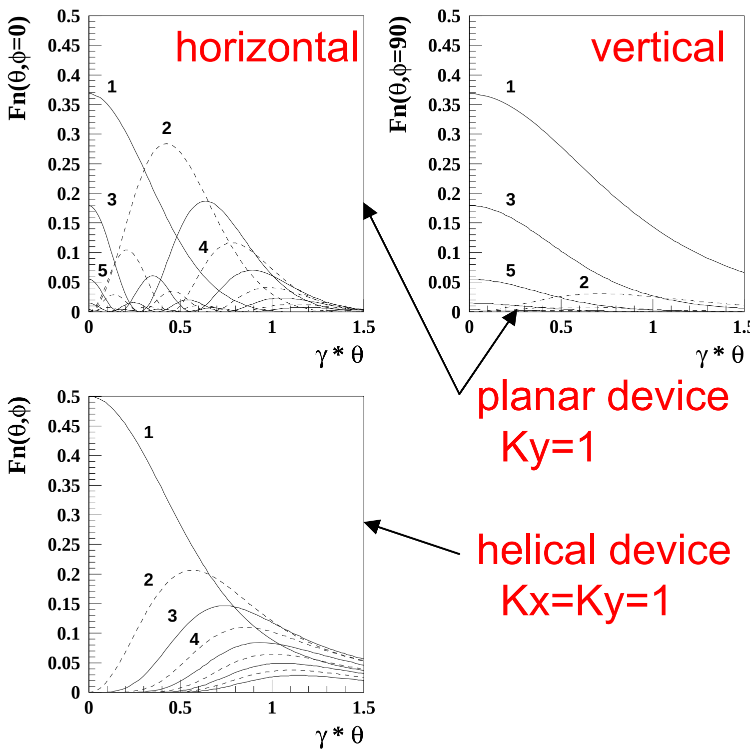

line shape function

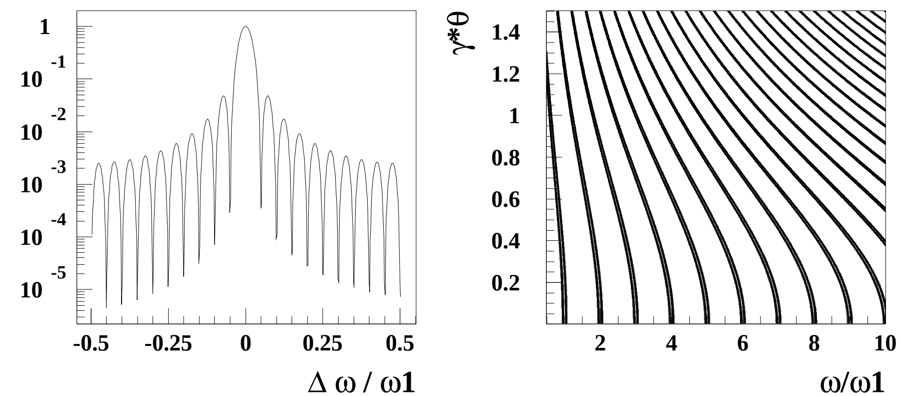

The angular divergence and the spectral width can be derived from the line shape function

divergence: $\sigma_{r'} = \sqrt{\lambda/2L}$

spectral width: $\frac{\Delta\omega}{\omega_n} = \frac{1}{nN}$

Useful Equations in Practical Units

on axis flux density of the nth harmonic (ph / s / mrad**2/ 0.1%BW)

$$\frac{\partial^2 \widetilde{F}}{\partial(\Delta\omega/\omega)\partial\Omega} = 1.744\cdot 10^{14}\cdot N^2\cdot E^2(GeV)\cdot I(A)\cdot F_n(K)$$

flux inside the central cone (ph / s / mrad**2/ 0.1%BW)

$$\frac{\partial \widetilde{F}}{\partial(\Delta\omega/\omega)} = 1.431\cdot 10^{14}\cdot N\cdot I(A)\cdot Q_n(K)$$

$$Q_n(K) = (1+K^2/2)\cdot F_n/n$$

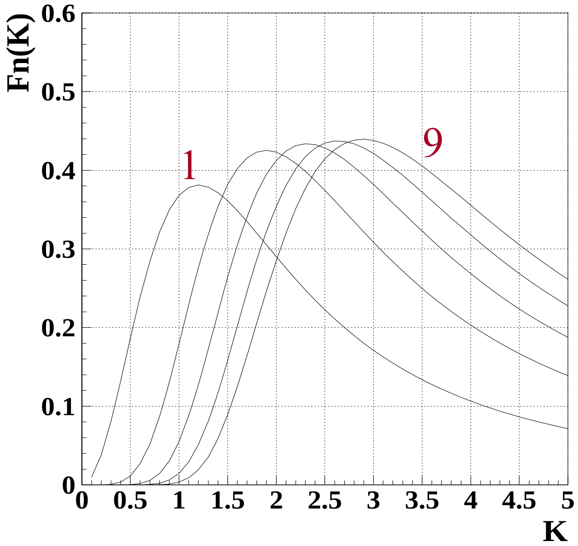

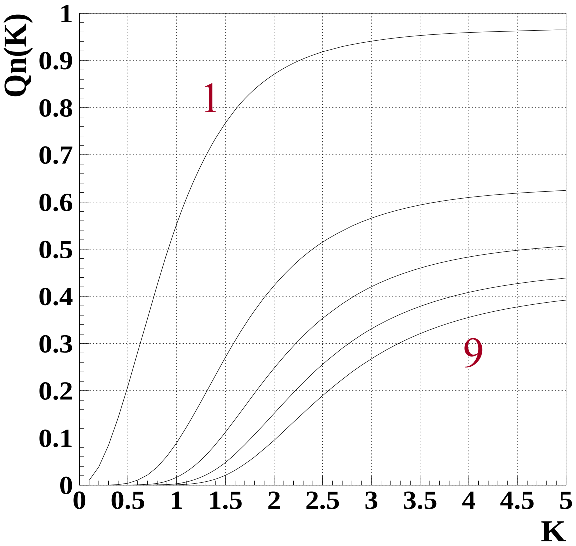

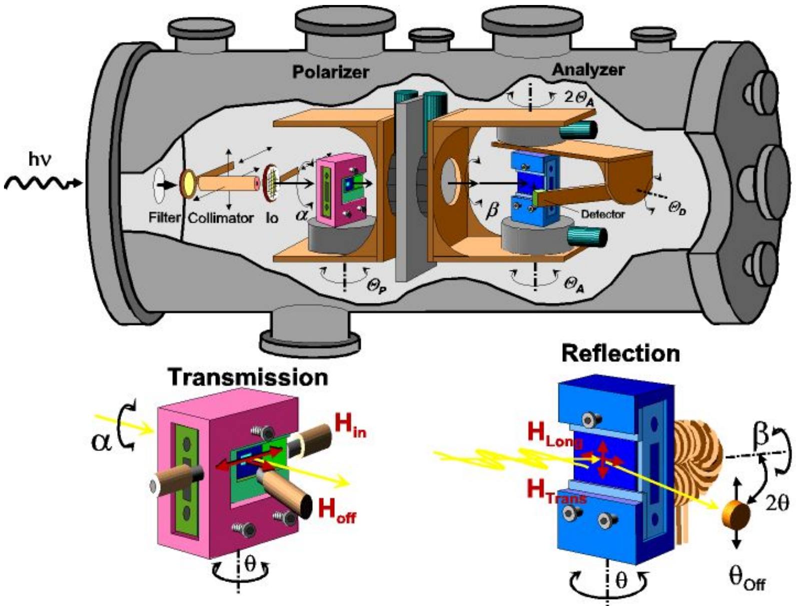

elliptical mode

inclined mode

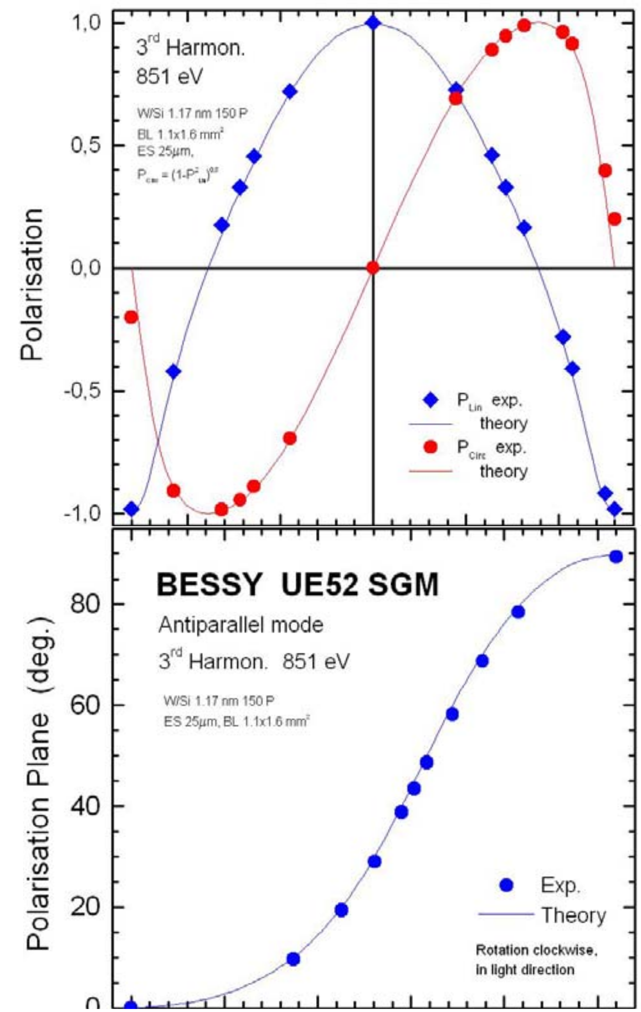

0 undulator phase π

The BESSY II Soft X-ray polarimeter

We observe excellent agreement between simulations and measurement

Difference between Wigglers and Undulators

Undulator parameter $K = 93.4 \cdot \lambda_0(m) \cdot B_0(T)$

horizontal divergence: K / γ

vertical divergence: $1 / \gamma$

ratio: K

wiggler: $K >> 1$

there is, however, no principle difference between undulators and wigglers

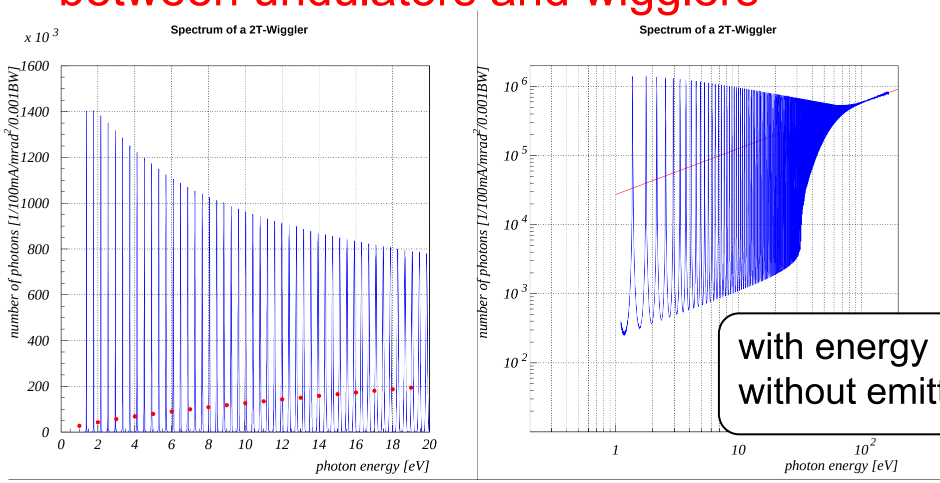

wiggler spectrum

corresponding dipole spectrum

radiation phase space is more compact for small K-values

7 Tesla Wiggler

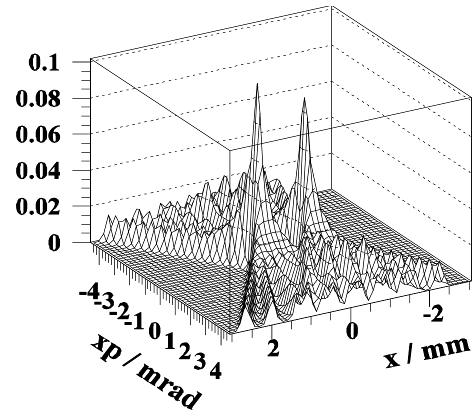

Undulator

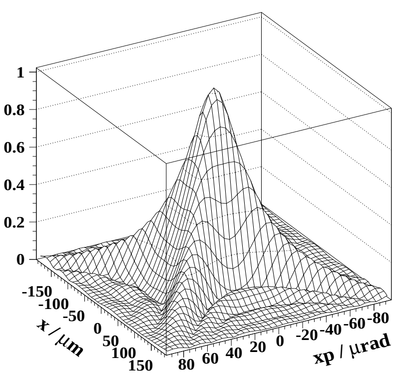

Undulator errors

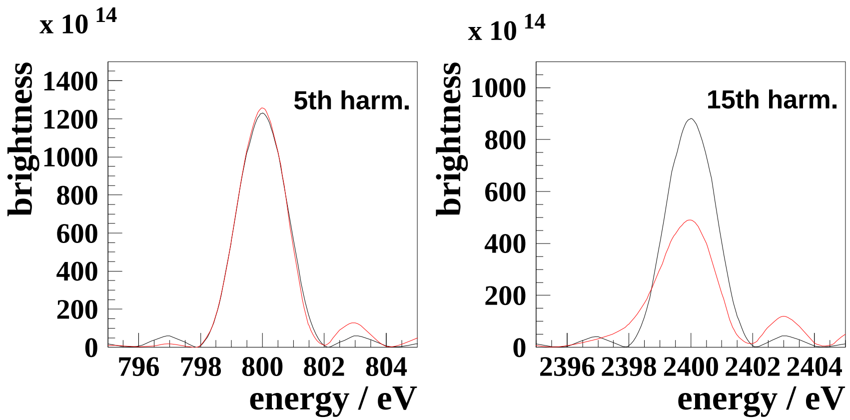

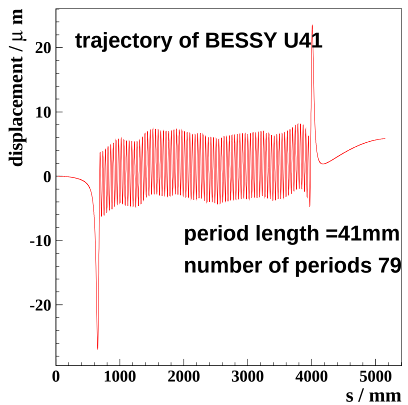

Phase error U41:
$\Delta\Phi$ (rms) = 2.6°

reduction of on axis flux density (Walker):

$$R = \exp(-\sigma_\Phi^2 n^2)$$

phase error from measured fields:

$$\Delta\Phi = \frac{2\pi}{\beta\lambda(B\rho)^2}\cdot\int_0^z\left[\int_0^{z'} B_y^{fit}dz''\cdot\int_0^{z'} B_y^{res}dz''\right]\cdot dz' + 0.5\cdot\frac{2\pi}{\beta\lambda(B\rho)^2}\cdot\int_0^z\left[\int_0^{z'} B_y^{res}dz''\cdot\int_0^{z'} B_y^{res}dz''\right]\cdot dz'$$

Beam parameters of a typical 3rd generation light source

beam emittance: 6 x $10^{-9}\pi$ m rad
β_x = 0.94 m
β_y = 2.1 m
energy spread: 8 x 10^{-4}

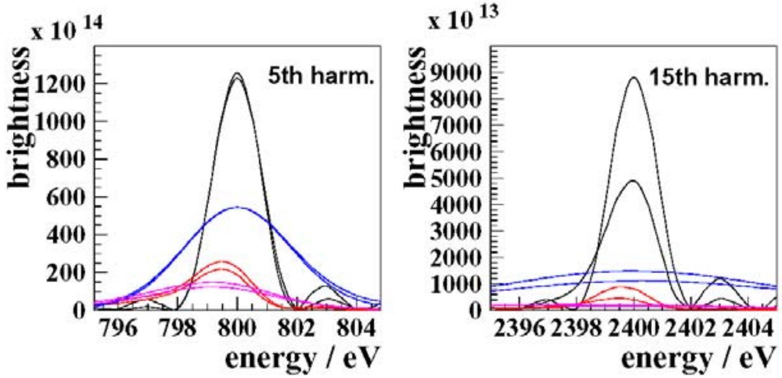

black: without emittance, energy spread
red: emittance included
blue: energy spread included
magenta: emittance and energy spread incl.

HELMHOLTZ ZENTRUM BERLIN für Materialien und Energie

Field optimization of undulators has two aspects:

1) *optimization of spectral performance*
today, spectral performance of undulators is limited by beam emittance and energy spread

2) *minimization of the interaction with the storage ring*
minimize static and dynamic multipoles

Methods:

1) *Magnet characterization and sorting before assembly*
2) *Minimization of optical phase error of magnet assembly*
3) *Compensation of static multipoles of magnet assembly*
   - Fe- shims
   - permanent magnet shims (increases minimum gap)
   - air coils at either end of the device (final compensation in SR)
4) *Compensation of dynamic multipoles of magnet assembly*
   - Fe-L-shims (suitable for APPLE in linear / elliptical mode)
   - flat wires glued onto the chamber (full flexibility for APPLE operation)

Magnet characterization and sorting minimizes shimming work after assembly
excellent agreement between predicted and measured fields integrals
for BESSY undulators UE52, UE49, UE112

longitudinal distribution
of field integrals

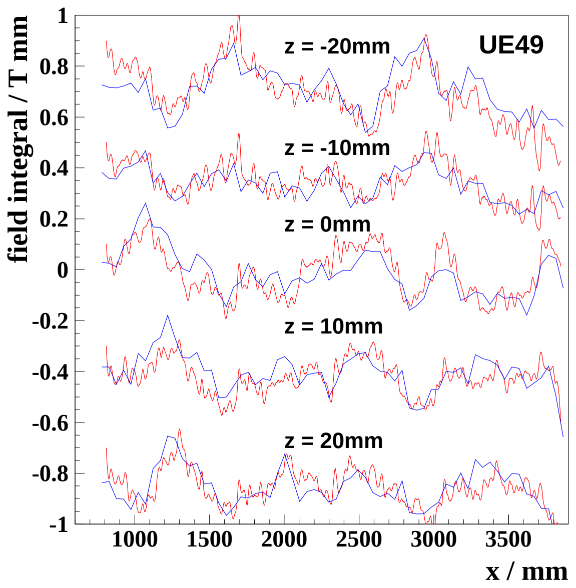

transverse distribution
of field integrals

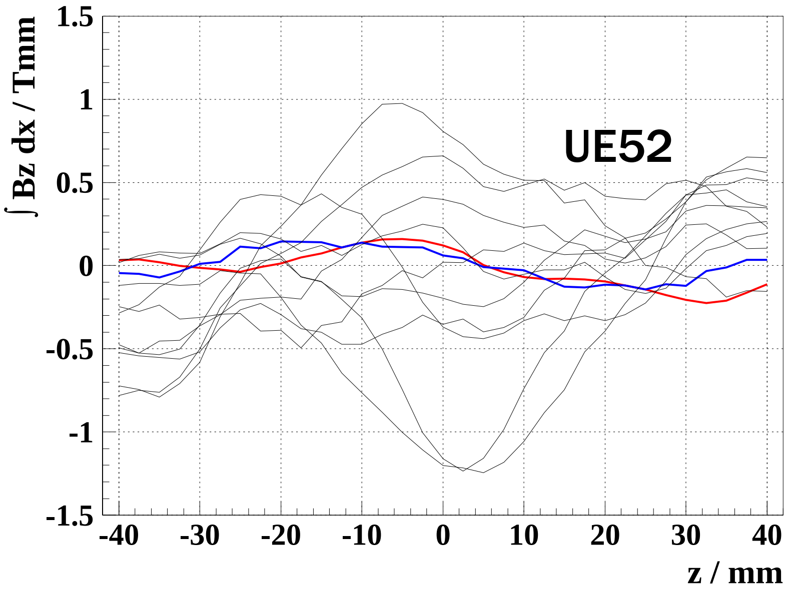

blue: prediction from single block measurements
red: Hall probe measurements

Local Field Measurements

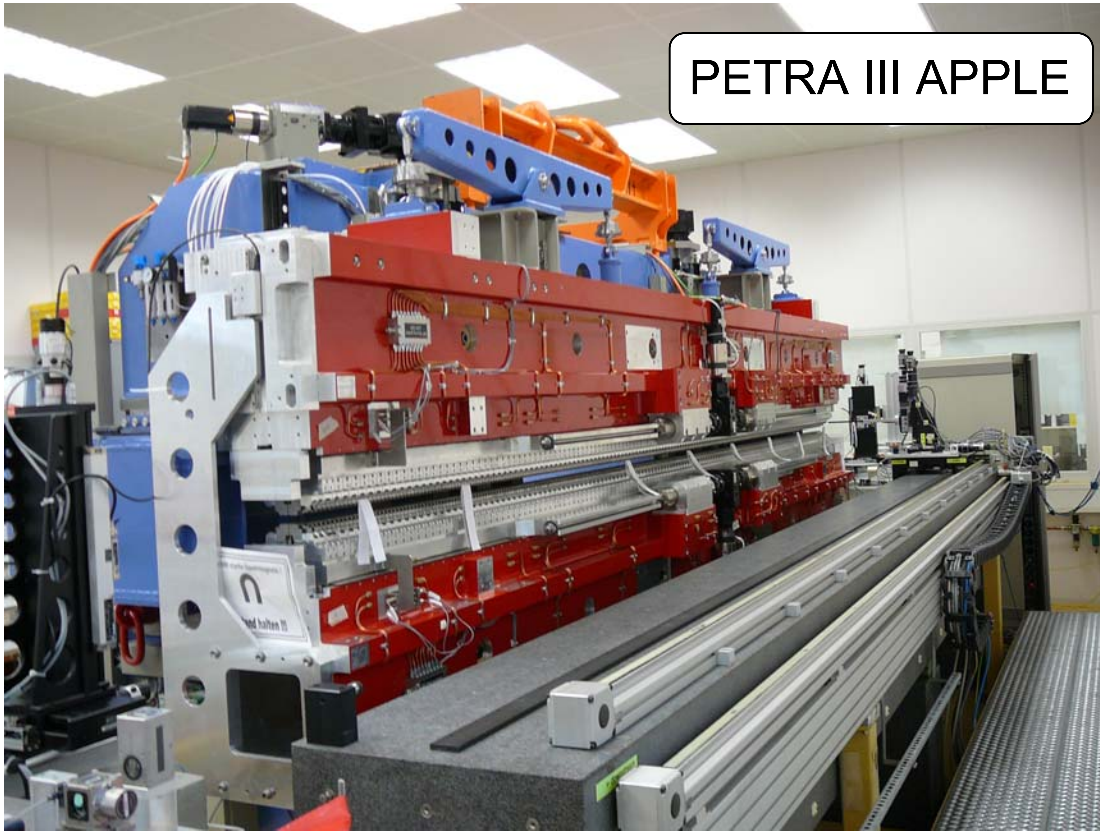

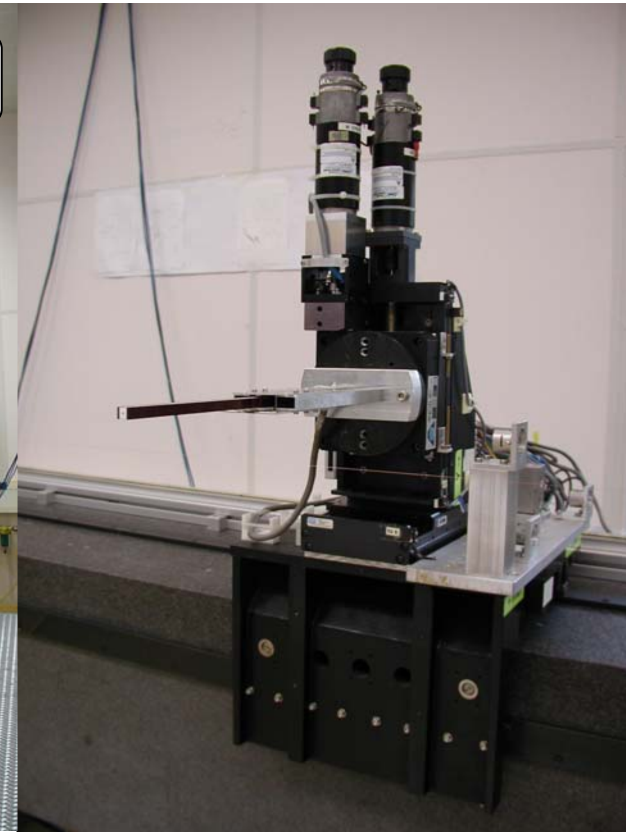

Granite bench: travel: 5.5 m x 100mm x 100mm
rms repeatibility of SENTRON Hall probes: 0.025 Tmm / 75 Tmm^2
(single measurement, 4min per scan)
alternative sensors: search coil, lambda coil, fluxgate sensor (small fields)

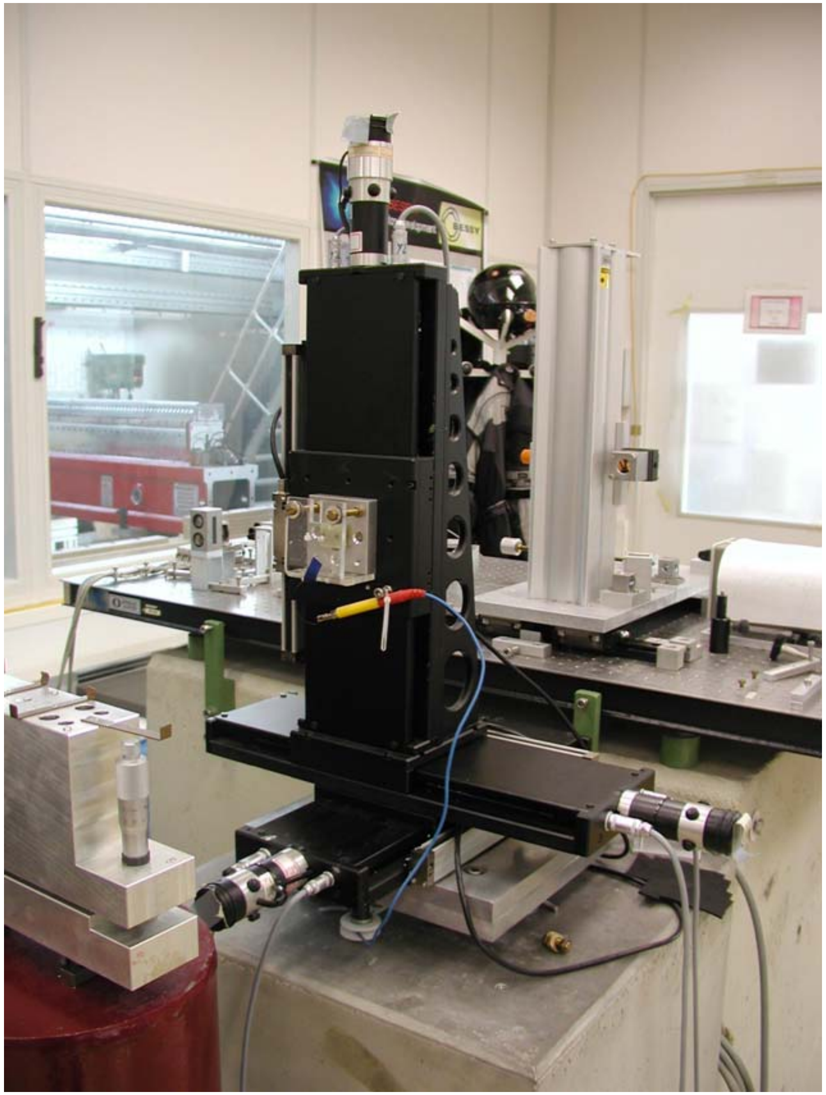

Moving wire system:
single wire, CuB Ø 125 µm
length: 6.5m
travel: 200mm x 200mm
rms repeatability: 0.003 Tmm
(single scan)
The system can be used also in a **pulsed wire** mode to detect the local distribution of first and second field integrals

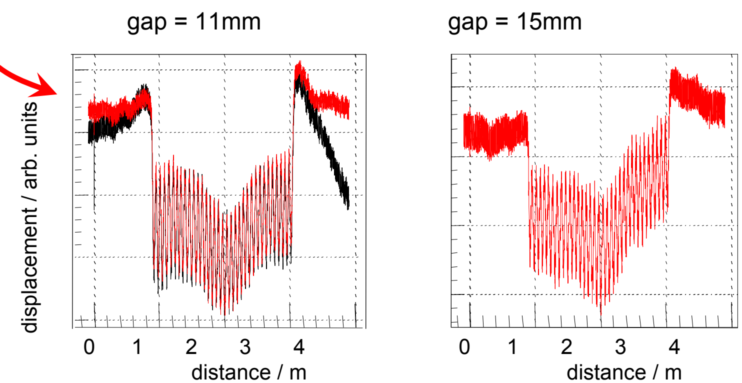

Correction coils not powered
Correction coils powered

trajectory straightening and phase shimming

method: virtual shimming (VS): horizontal and vertical block movement

VS introduces additional phase dependent field integrals

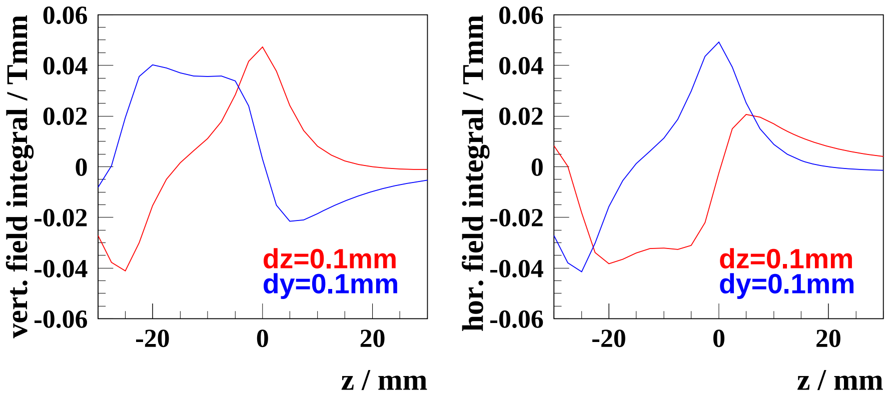

Field integrals as produced by virtual shimming

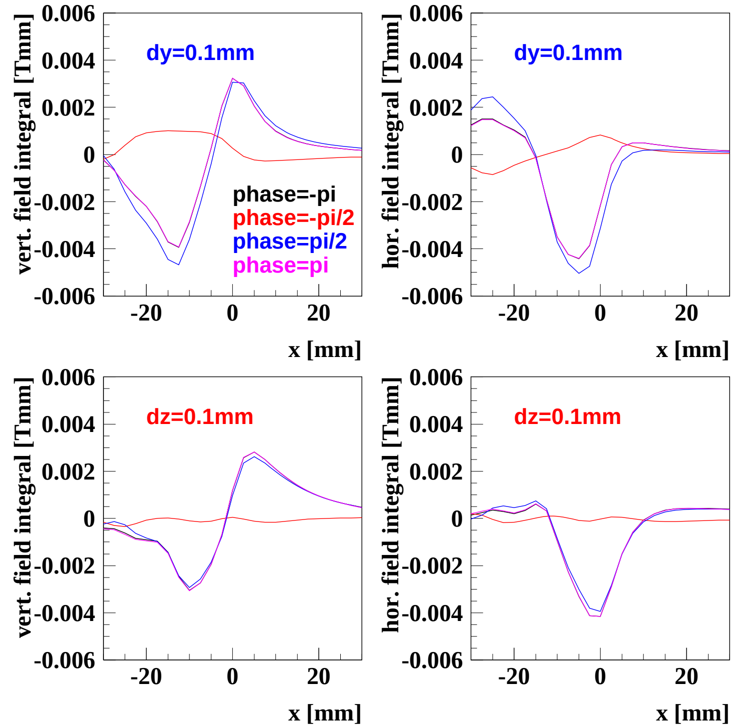

Phase dependent field integrals as produced by virtual shimming

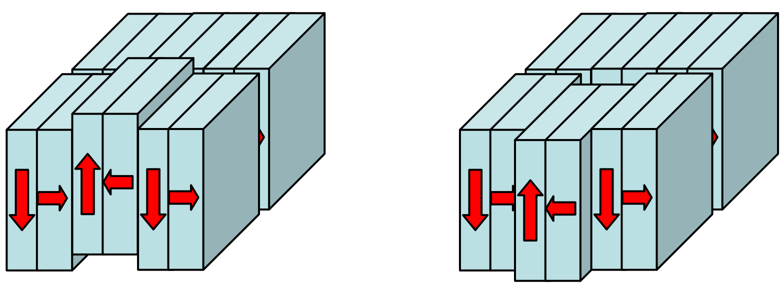

vertical movement (dy) horizontal movement (dz)

Field Optimization II: Application of Fe-Shims

HELMHOLTZ ZENTRUM BERLIN für Materialien und Energie

shimming of phase dependent field integrals

method: Fe-shims with phase dependent response

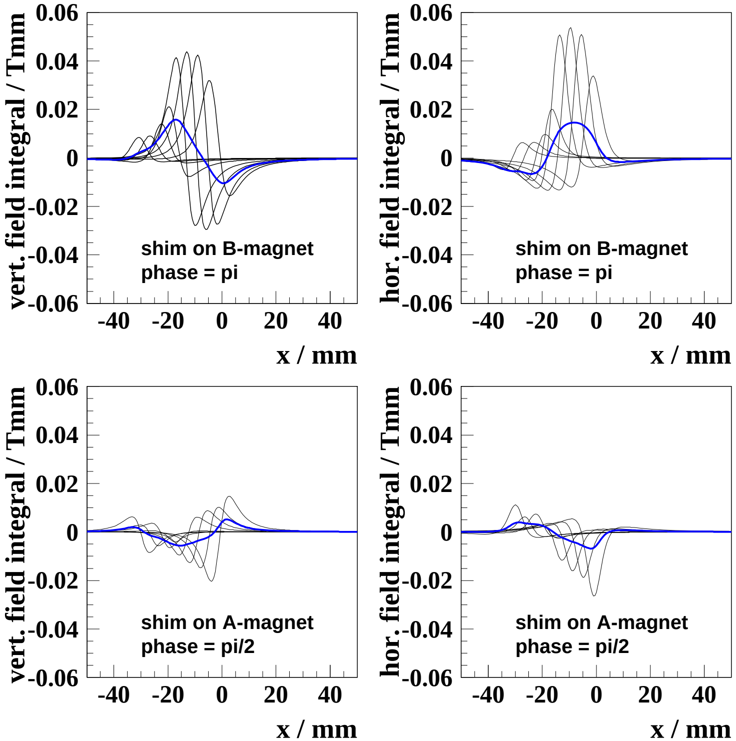

shim response of Fe-shims
on APPLE undulator magnets

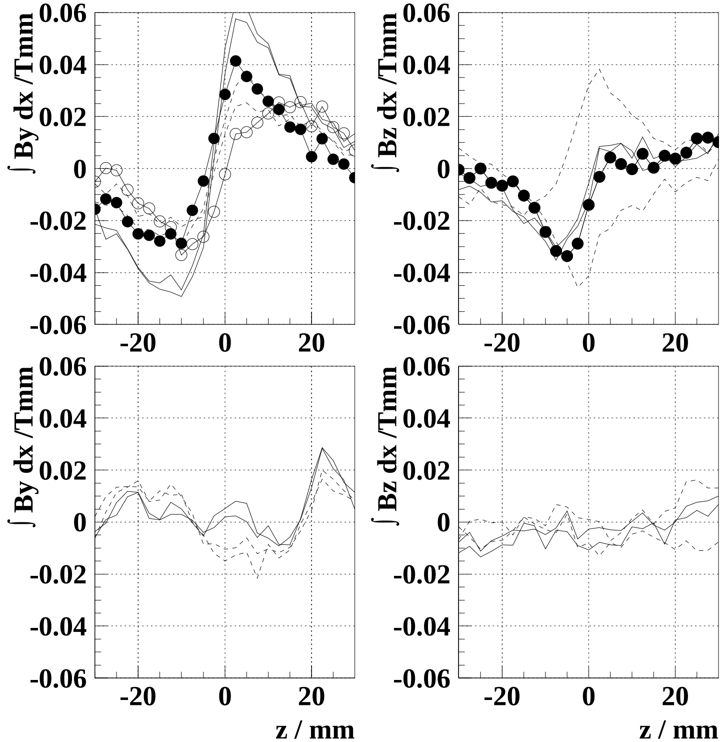

phases:
dashed:
±λ/4
solid:
±λ/2

field integrals before (top)
and after (bottom) shimming

J. Bahrdt et al, Nucl. Instr. and Meth, in Phys. Res. A 516 (2004) 575-585

Field Optimization III: Tuning of Magic Finger

shimming of shift independent field integrals with permanent magnets

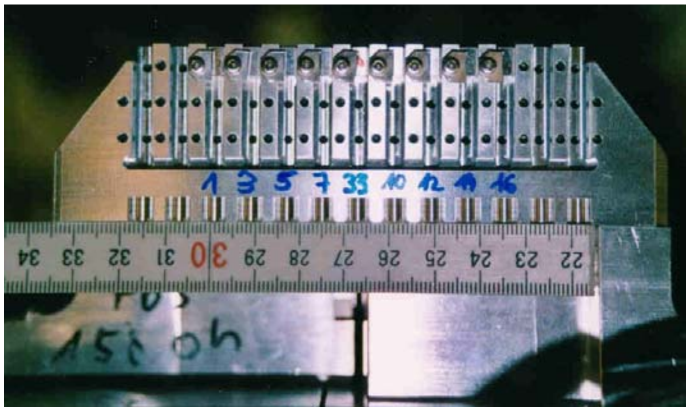

BESSY
standard
magic finger

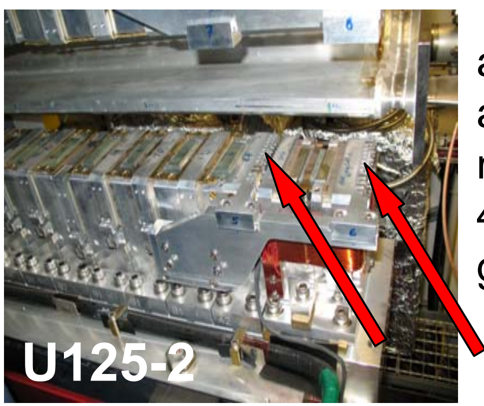

arrays of permanent magnets at either end of the device
magnet dimensions:
4x4 mm^2, variable thickness,
grid size 4mm

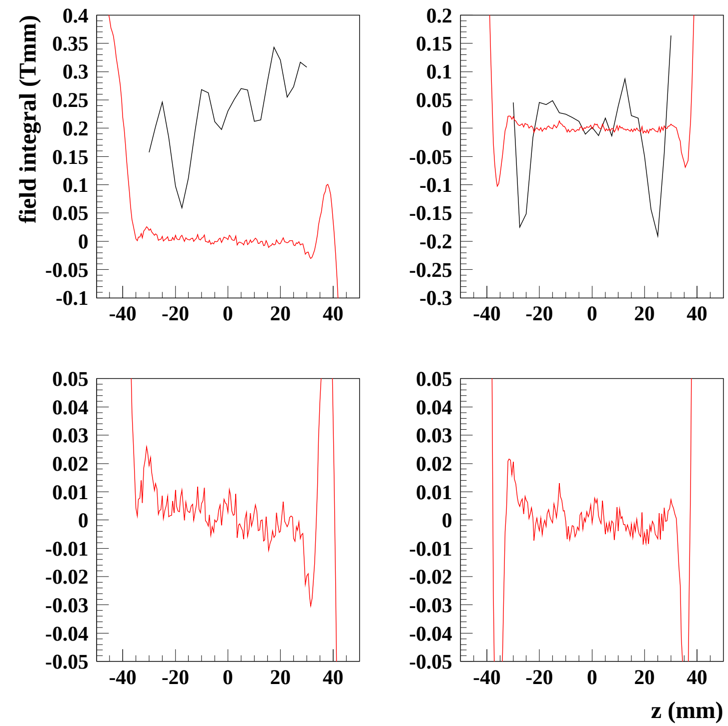

BESSY II U125-2
black: without MF
red: with MF

Field Optimization IV: Pole Height Adjustment

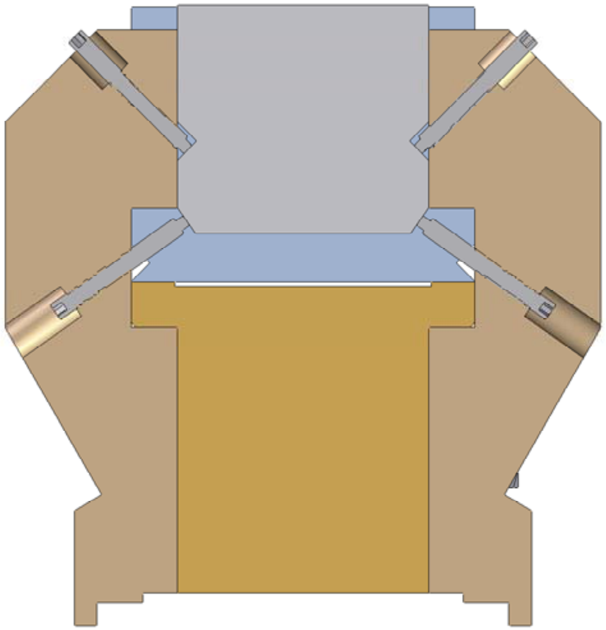

Shimming of vertical field errors:

→ vertical pole movement

Shimming of horizontal field errors:

→ pole tilt

Adjustment Range:

Pole Height : ± 0.3mm

Pole Tilt : ± 1mrad

J. Pflüger, H. Lu, T. Teichmann NIM A429 (1999), 368

Courtesy of J. Pflüger, XFEL

Successfully applied to FLASH and PETRA III undulators

Classification of permanent magnet undulators

Spacing of undulator spectral harmonics
- equally spaced: periodic undulator
- non equally spaced: quasiperiodic undulator

On axis radiation power
high power on axis: planar undulator
reduced power on axis: helical, figure 8 undulator

Polarization
fixed poarization
- planar device for linear polarization
- helical device for circular polarization

variable polarization
- hor. and vert. lin. and elliptical
- additionally variable angle of linear polarization
- arbitrary polarization

Clean Spectra: Quasiperiodic Undulators (S. Sasaki)

generate 1D-quasiperiodic lattice

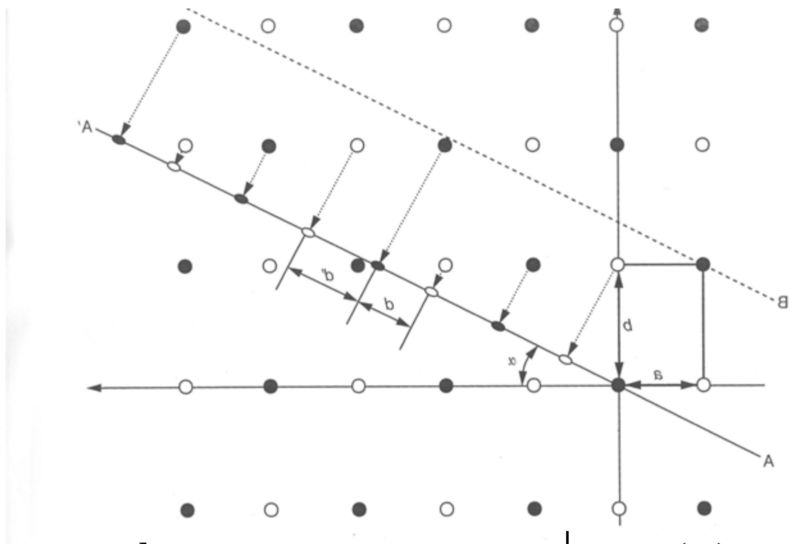

$$z_m = \frac{d}{r \cdot \tan(\alpha)} \cdot \left(m + (r \cdot \tan(\alpha) - 1)\left\lfloor \frac{\tan(\alpha)}{r + \tan(\alpha)} m + 1 \right\rfloor\right)$$

$$r = b / a$$

original design

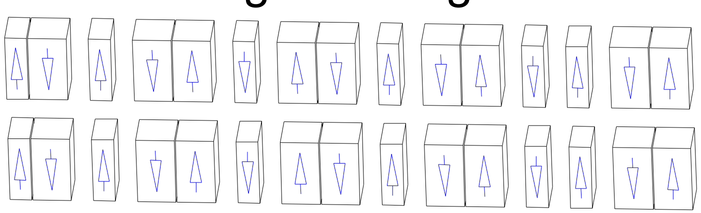

ESRF / ELETTRA design

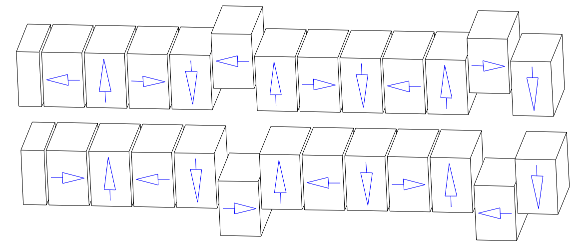

BESSY II design

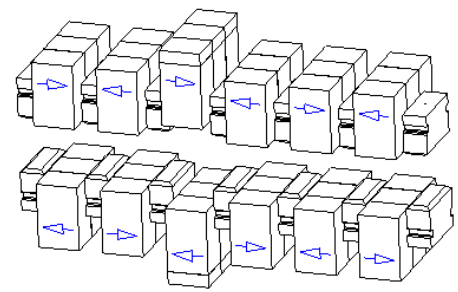

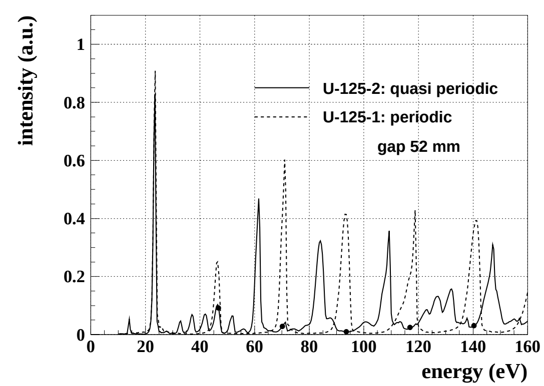

spectra derived from measured magn. fields

Reduced On-axis Flux Density Designs

$$\frac{\partial P}{\partial \Omega}(W/mrad^2) = 0.01344 \cdot E(GeV)^2 \cdot I(A) \cdot N \cdot \int_{-\lambda_0/2}^{\lambda_0/2} \left[\frac{\upsilon_x'^2 + \upsilon_y'^2}{D^3} - \frac{((\upsilon_x^2)' + (\upsilon_y^2)')^2}{D^5} \right] \cdot ds$$

$$D = 1 + \upsilon_x^2 + \upsilon_y^2$$

$$\upsilon_{x/y} = \gamma(\beta_{x/y} - \theta_{x/y})$$

High on axis power density
planar device, K=4

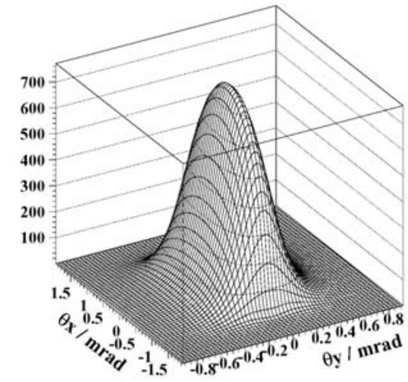

example: angular flux density for:
energy=1.7GeV, current=0.1A,
N=100, λ = 50mm
Kx/Ky=0, 0.25, 0.5, 0.75, 1.0

low on axis power density
helical device, Keff=4 figure-8 undulator

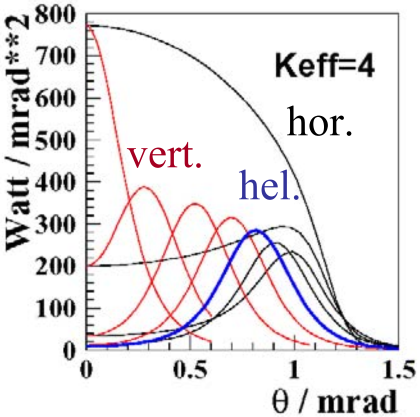

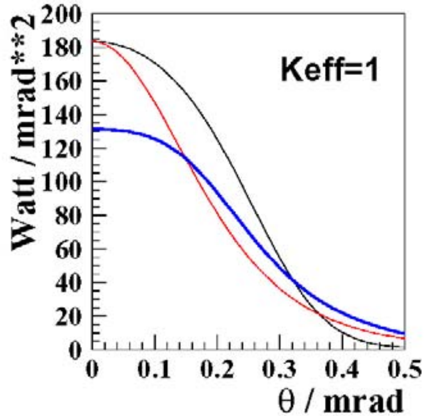

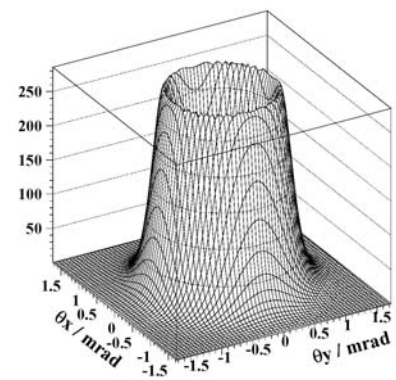

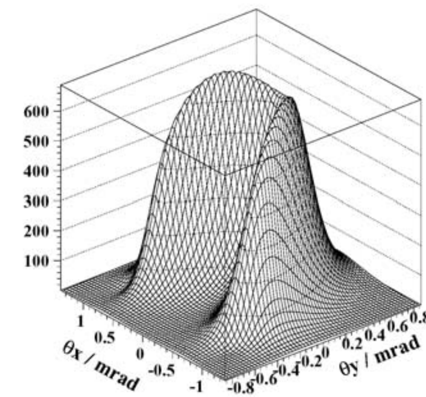

Elliptically Polarizing Undulators I

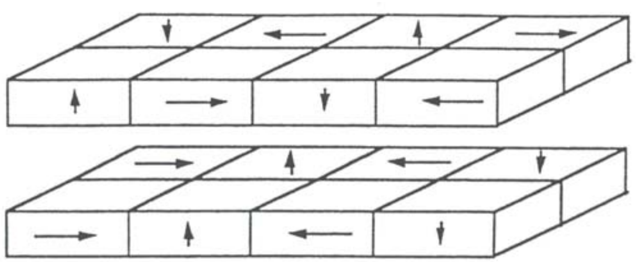

ESRF
(+) variable polrization
  upper beam: vert. field
  lower beam: hor. Field
(-) vertical steering
(-) medium fields

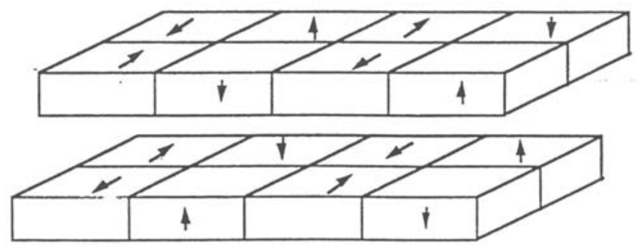

ELETTRA
(+) helical, independent
  on gap setting
(-) medium fields
(-) no further
  polarization modes
(-) narrow good field
  region

SPRING-8
(+) variable
  polarization
(+) larger good field
  region
(-) week fields
(-) mechanically
  complicated

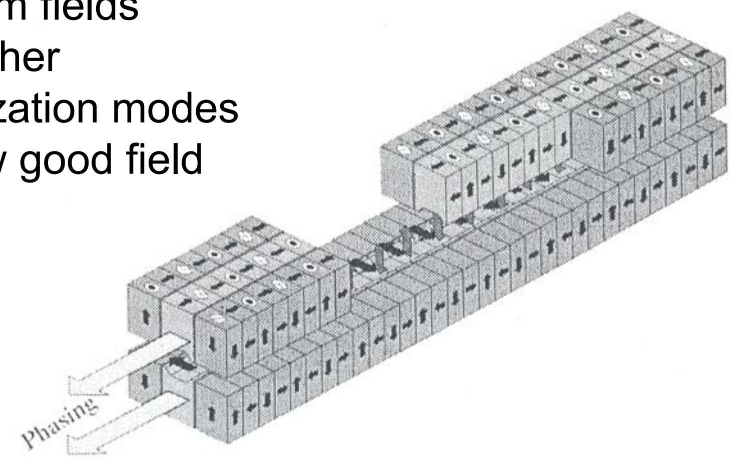

APPLE II, Advanced Polarizing Photon Light Emitter

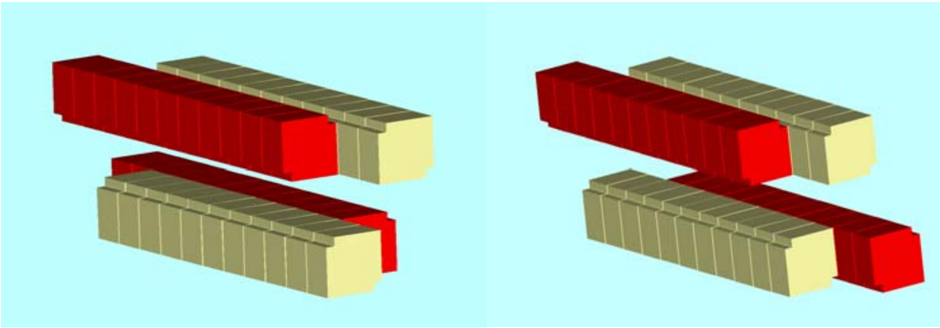

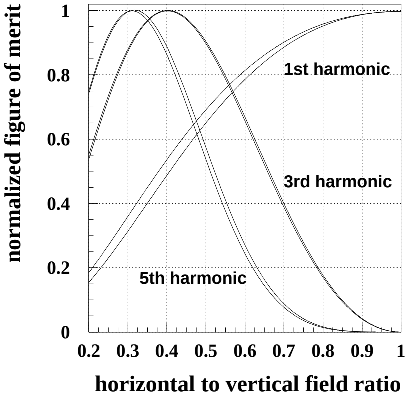

- (+) highest fields
- (+) full flexibility e.g. APU
- (-) mechanically complicated
- (-) narrow good field region

relative phase of By, Bz defines ellipticity

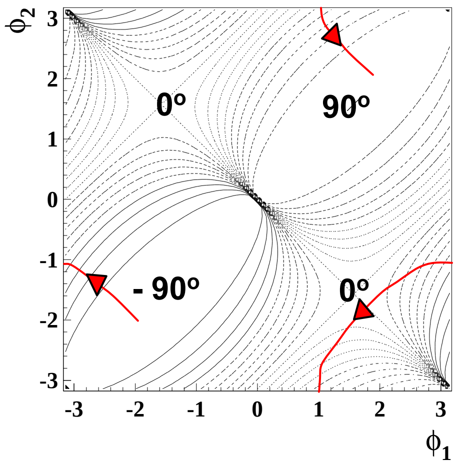

ratio By / Bz defines inclination

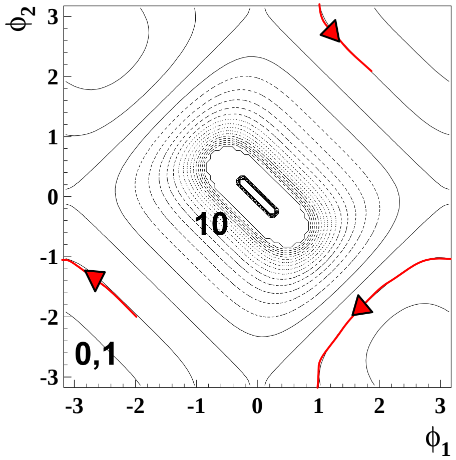

effective field

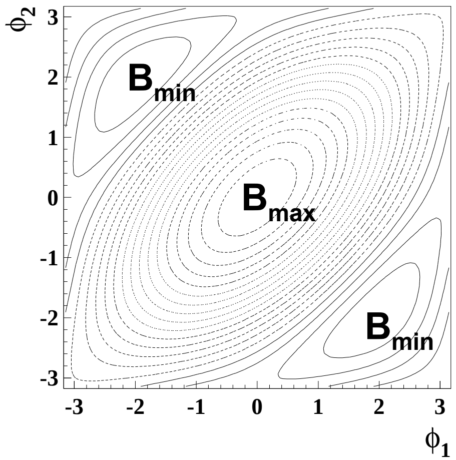

Geometric Tolerances

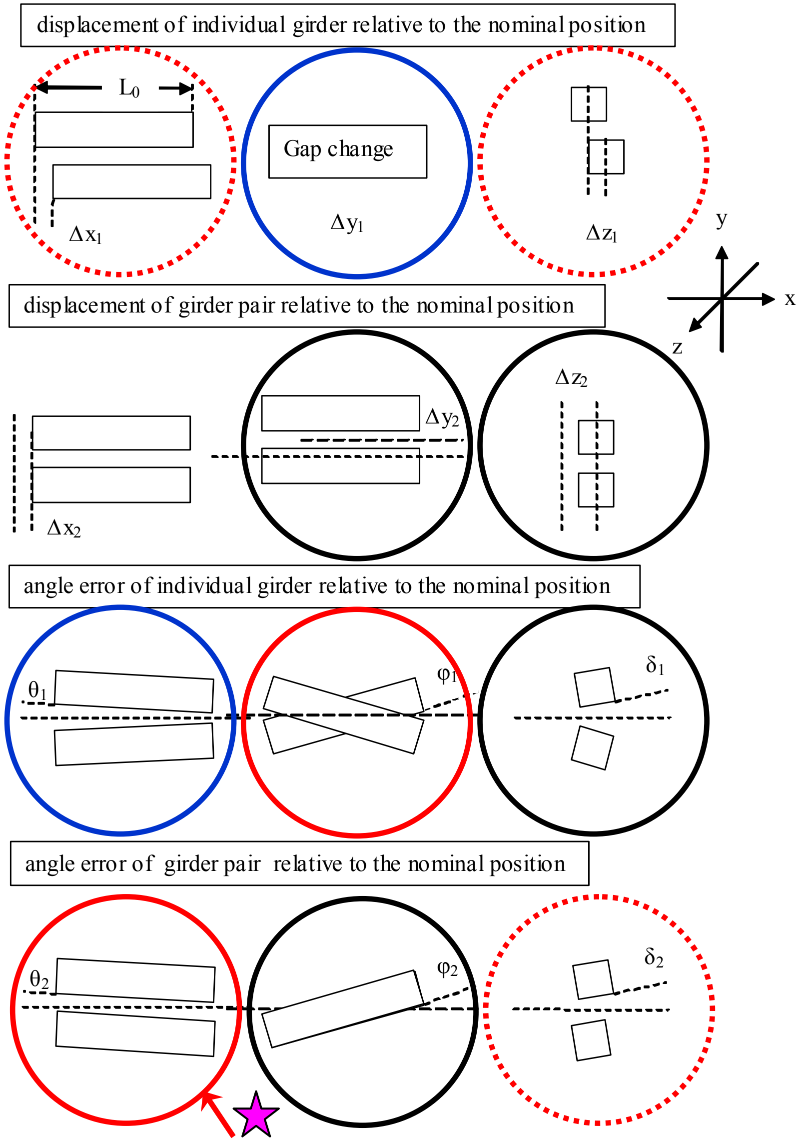

black: independent on forces
accuracy and stiffness of of support structure

blue: **closed loop servo systems**

red, dotted: dependent on forces
appears in inclined mode
produces K-shift
stiff support structure

red, solid: dependent on forces
appears in inclined mode
produces ☟K/K-shift
★ **feed back compensation using 4 motors**

Stiff Design: Cast Iron Support Structure

HELMHOLTZ ZENTRUM BERLIN für Materialien und Energie

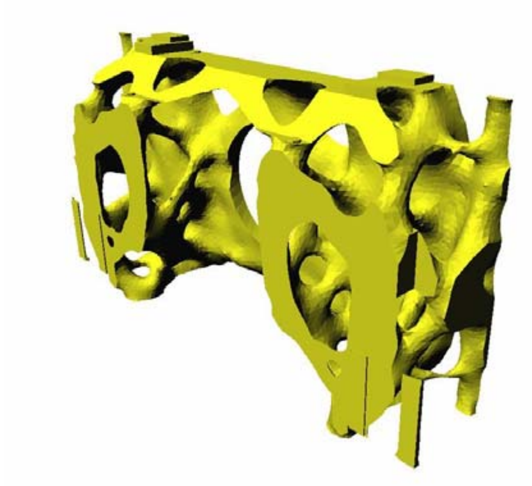

bionic optimization

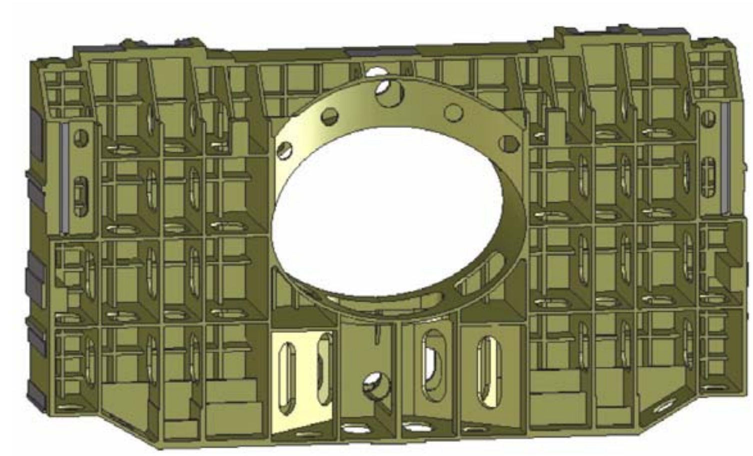

Stiff Design: Magnet Girder

Magnet girder

material: cast Aluminum
length: 5m
single piece of Al

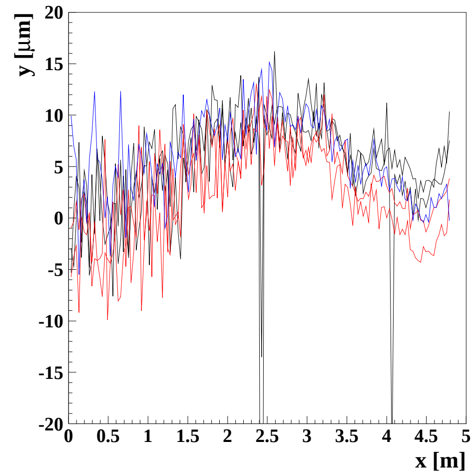

Laser interferometer measurements at HZB:
Straightness: 10µm over 5m

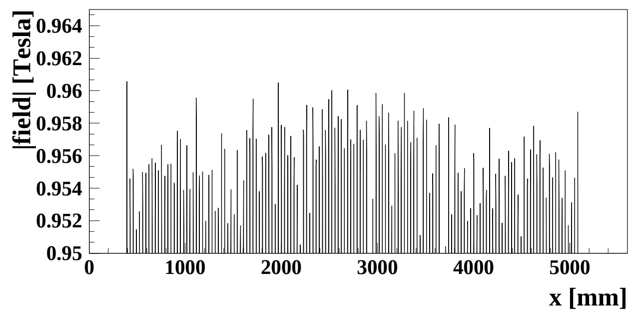

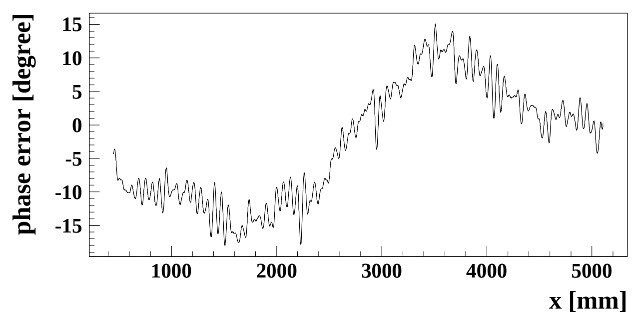

phase error for phase = pi is dominated by geometric error of girder

→ simple compensation with spacers

Gap Positioning Accuracy

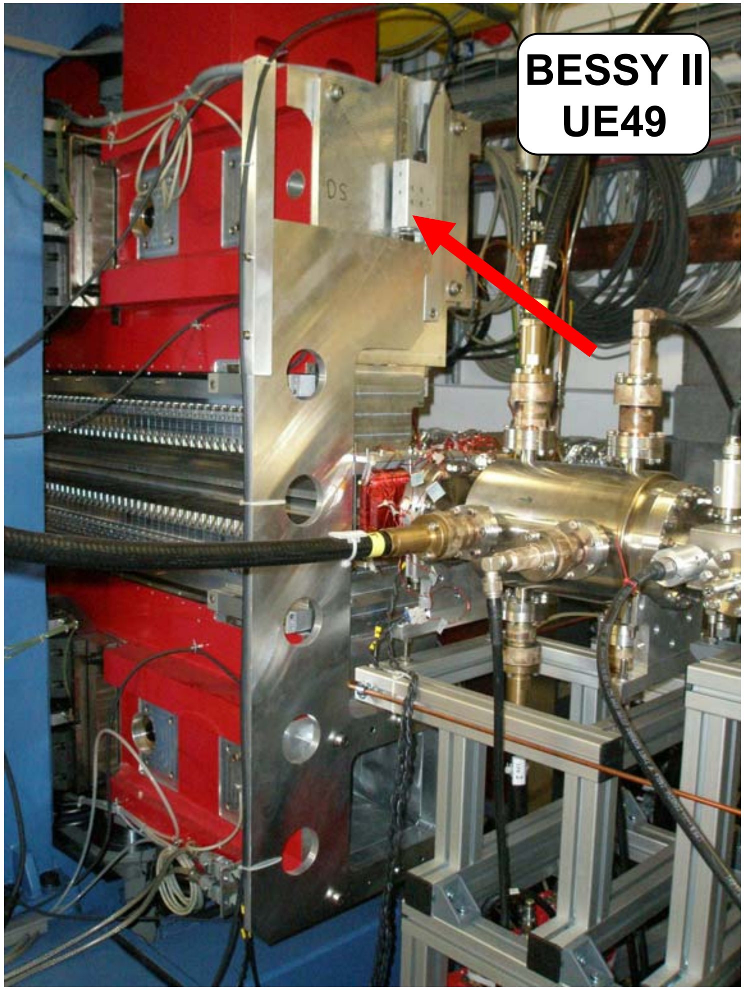

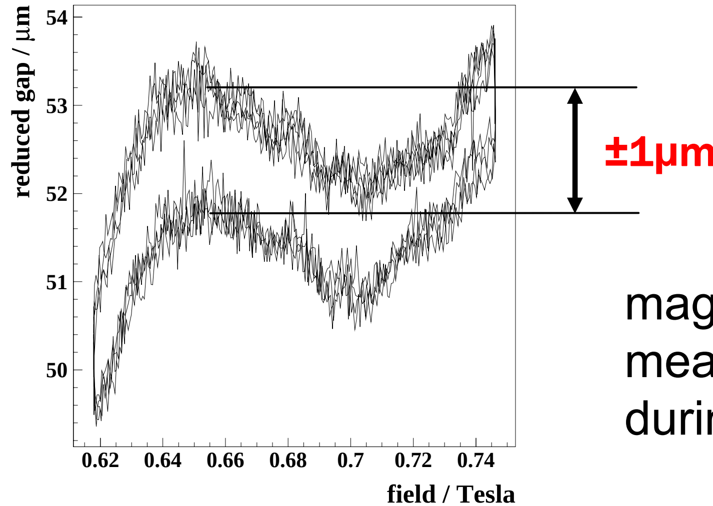

magnetic field measurement during gap drive

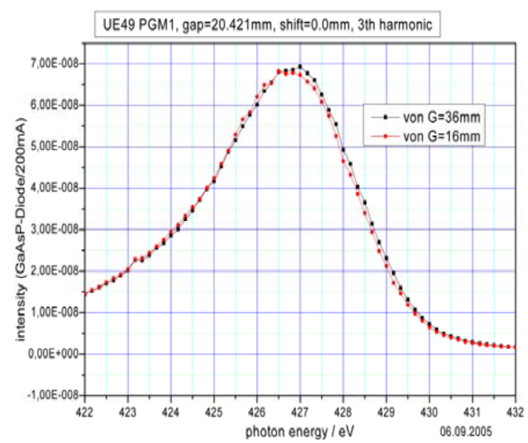

measured spectra for different directions of gap drive

BESSY II Double Undulator for Fast Helicity Switching

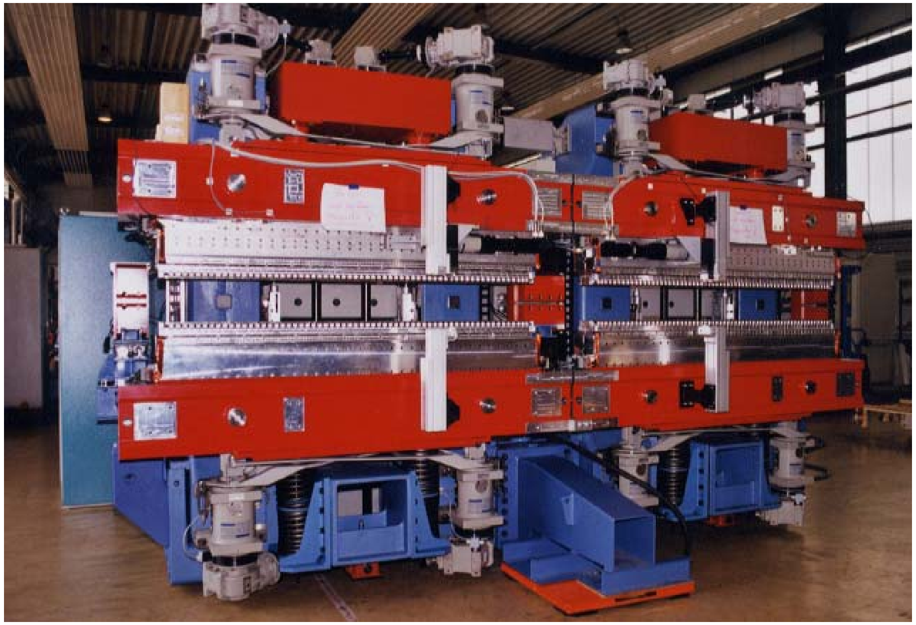

Modulator Mode

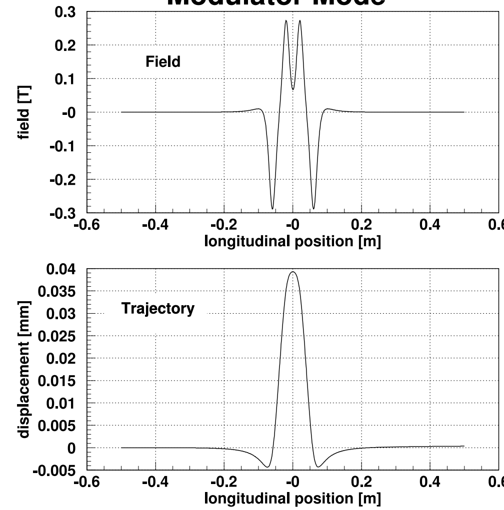

BESSY II UE56 double undulator (top) and permanent magnet modulator / chicane (left)

J. Bahrdt et al., SRI2000

Chicane Mode

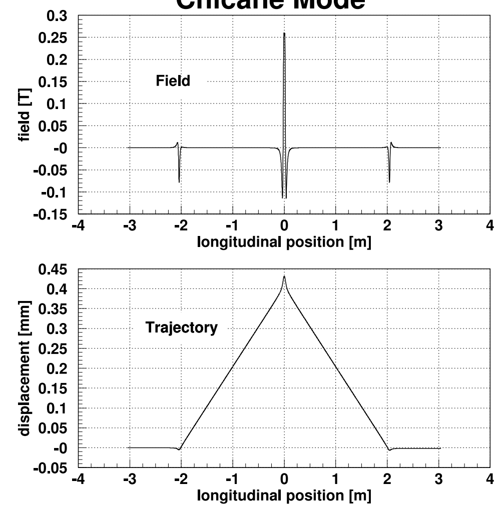

PETRA III APPLE Currently Built at HZB

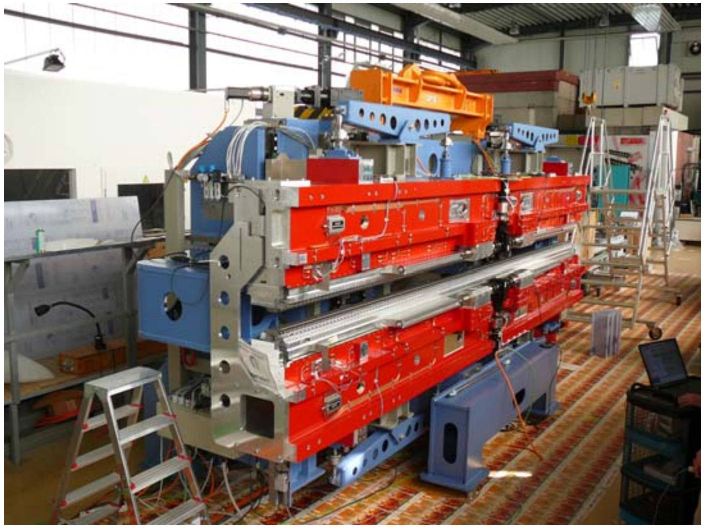

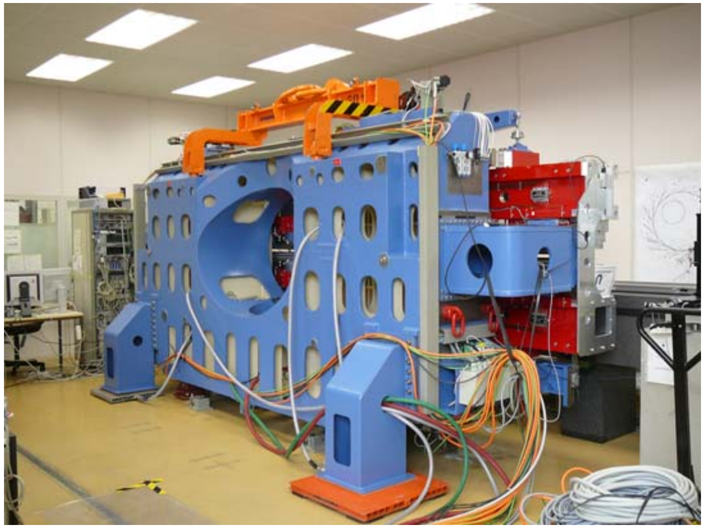

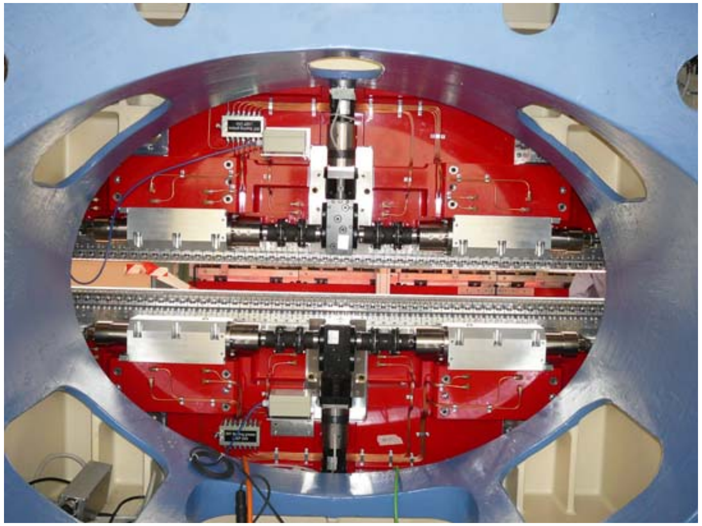

total length: 5m
weight: 18to
\# of magnets: 1200
maximum force: 70 kN

- full polarization control via four phase motors
- independent drive systems for lower girder and gap motion

HELMHOLTZ ZENTRUM BERLIN für Materialien und Energie

APPLE III design:
factor 1.4 higher field as compared to APPLE II

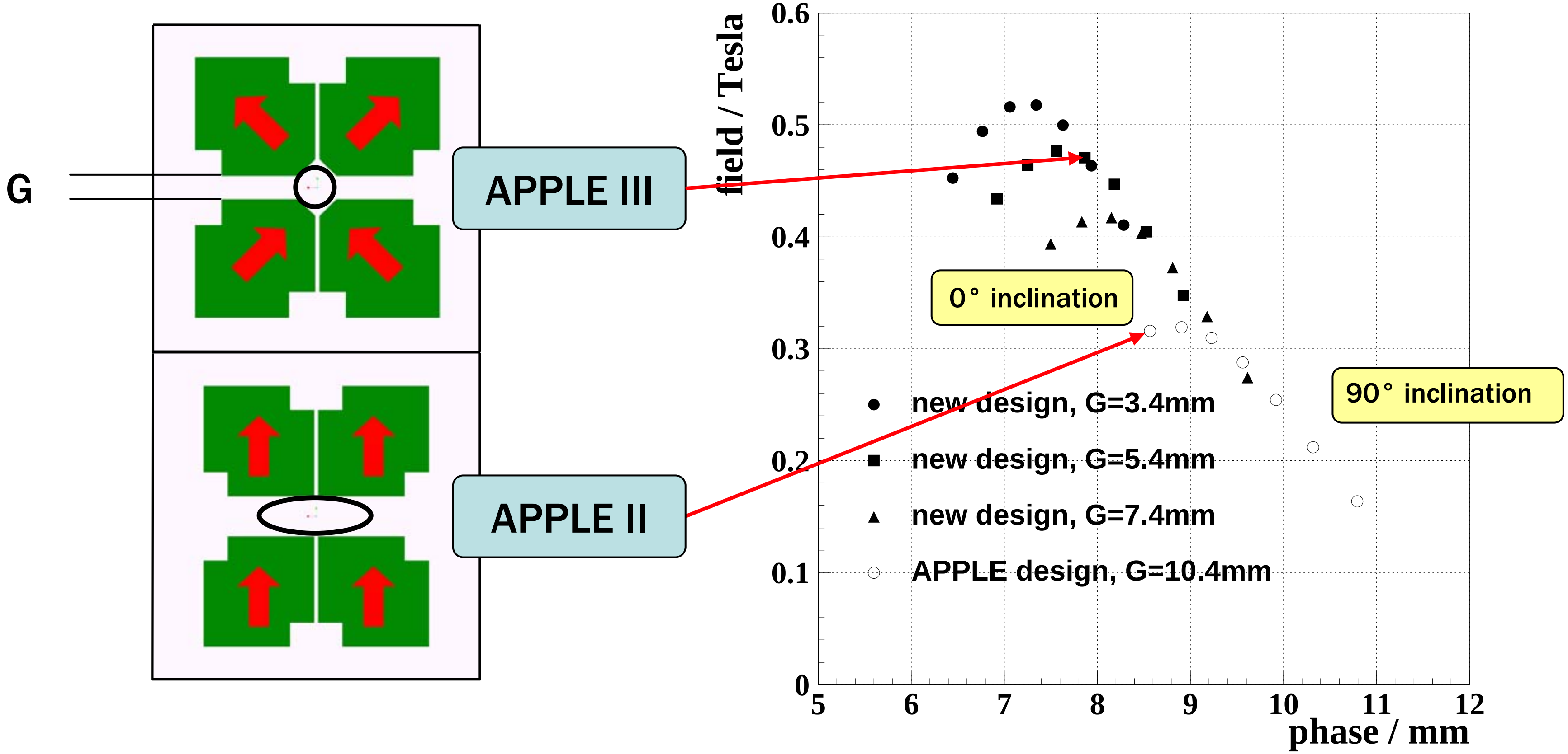

J. Bahrdt et al., Proceedings of the 26th International FEL Conference, Trieste, Italy, 2004, pp610-613

Elliptically Polarizing Undulators IV

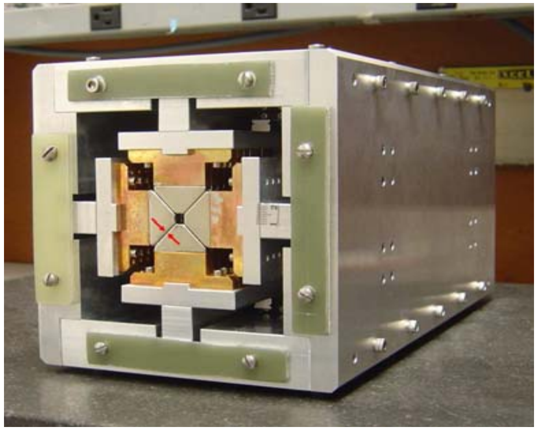

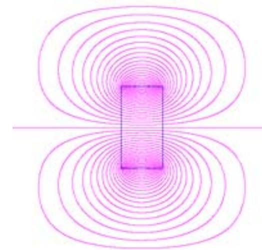

Single NdFeB (40SH) PM block,
T_demag ~ 132degC

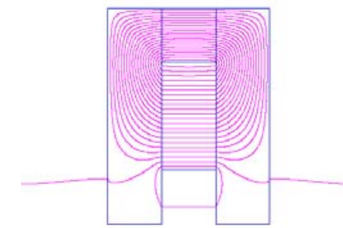

PM block in steel jacket
T_demag ~ 228degC !

length: 300mm
inner diameter: 5mm
slit between arrays: 0.5mm

A. Temnykh, PRST-AB, 11, 120702 (2008)

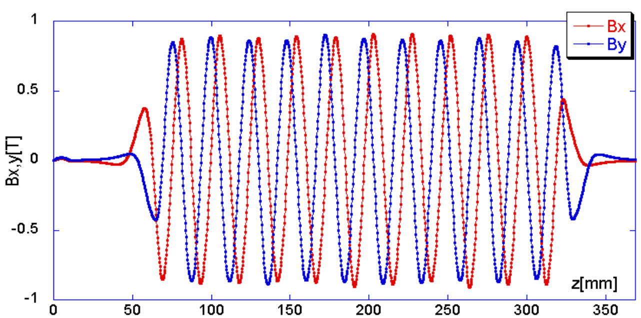

Measured fields of Delta undulator

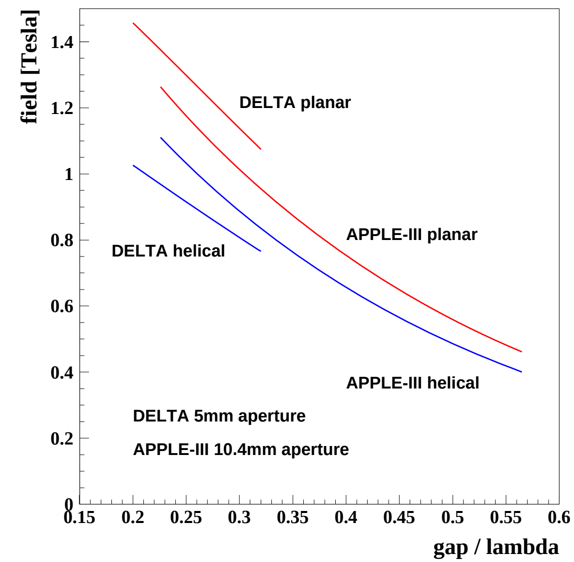

Comparison of
DELTA and APPLE III ID

Higher Photon Energies: In Vacuum Devices

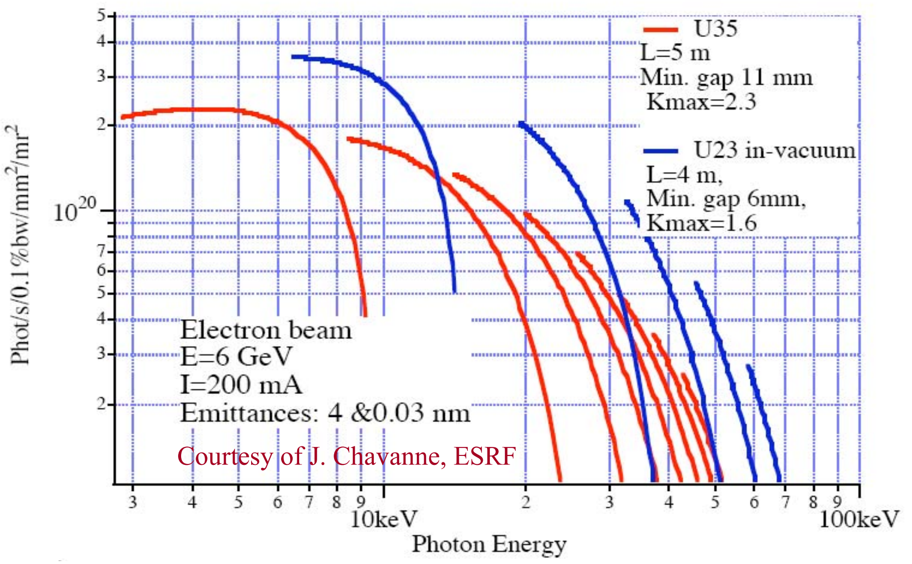

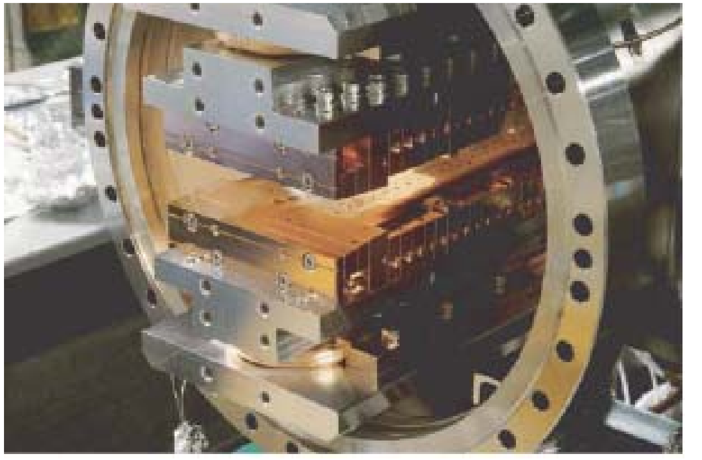

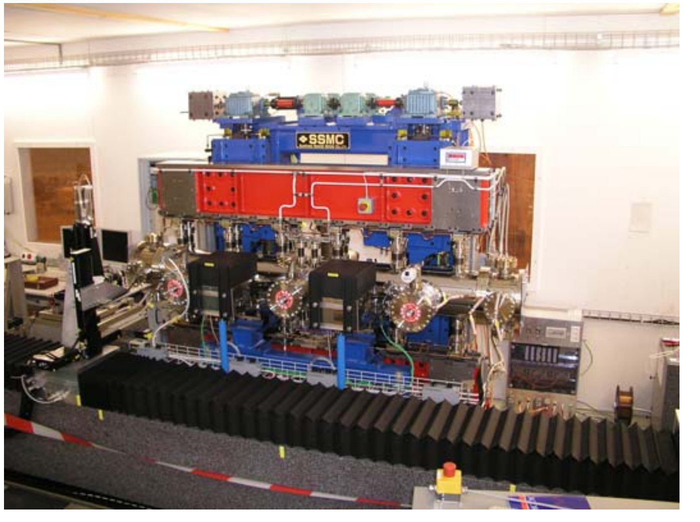

SLS U19 In-Vacuum Undulator

Courtesy of Th. Schmidt, SLS

Mechanically complicated but mature technique

- coating of magnets to reduce outgassing
  Ti+TiN ion plating of NdFeB magnets (SPRING8)
- high coercive magnetic material (bakeout at 125°)
- thin metal sheet to reduce image current heating
  (50 μm Ni + 10 μm Cu)
- water cooled RF-fingers
- special shimming techniques

In Vacuum Revolver

HELMHOLTZ ZENTRUM BERLIN für Materialien und Energie

SPRING 8

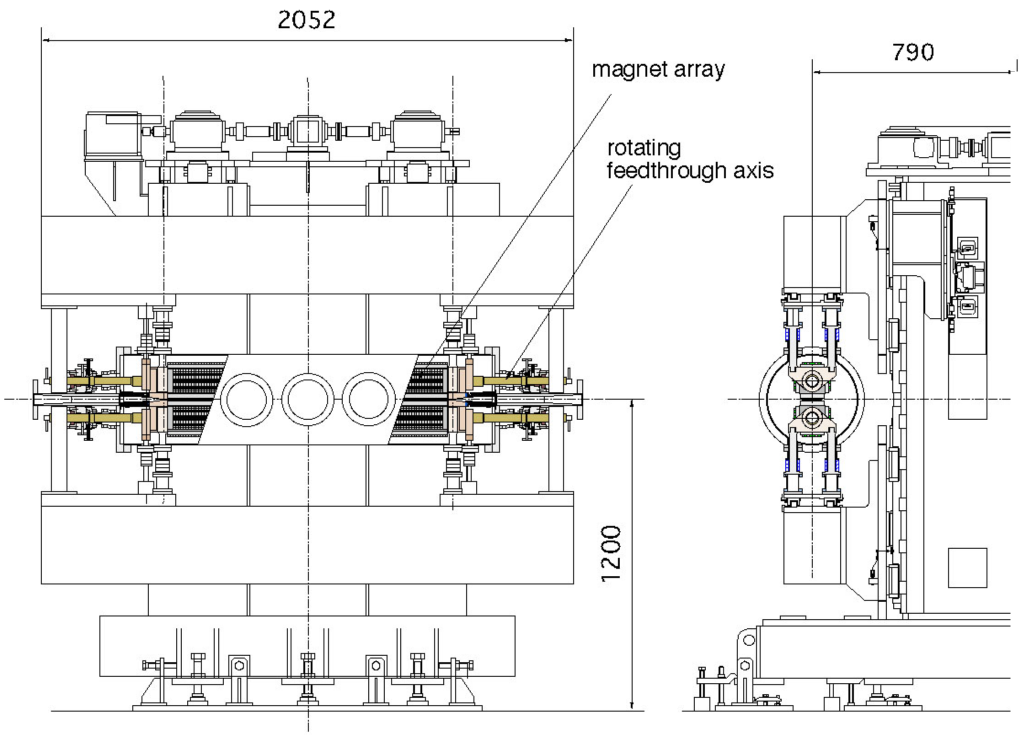

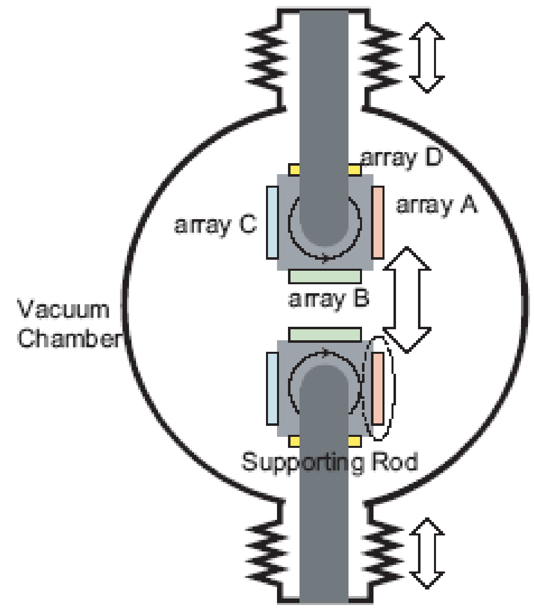

Covering a wide photon energy range with several devices which have slightly different period lengths: overlap of 1st & 3rd harm.

T. Bizen et al., AIP Conf. Proc. of SRI conference, Vol. 705 (2004) pp175-178.

second order kicks *(Elleaume, EPAC 1992):*

$$\theta_{x/y} = -\frac{1}{(B\rho)^2}\int\left\{\int B_x dz' \cdot \int \frac{\partial B_x}{\partial x/y} dz' + \int B_y dz' \cdot \int \frac{\partial B_y}{\partial x/y} dz'\right\} dz$$

$$\theta_{x/y} = -\frac{L}{2(B\rho)^2}\frac{\lambda_u^{\ 2}}{(2\pi)^2}\left\{B_x^0 \cdot \frac{\partial B_x^0}{\partial x/y} + B_y^0 \cdot \frac{\partial B_y^0}{\partial x/y}\right\}$$

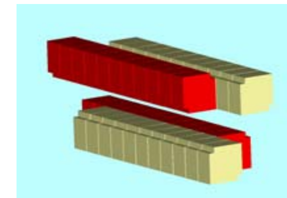

APPLE, elliptical mode

generic representation of second order kicks:

$$\theta_x(x) = f_0(x)\cos^2(\varphi/2) + f_\pi(x)\cdot\sin^2(\varphi/2) + f_{\pi/2}(x)\cdot\sin^2(\varphi)$$

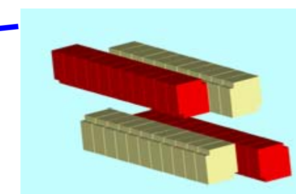

APPLE inclined mode

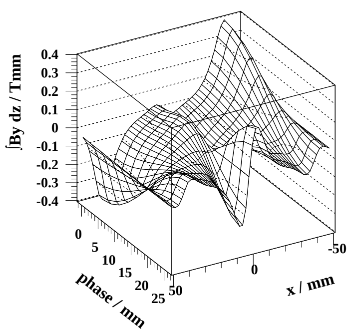

inclined mode

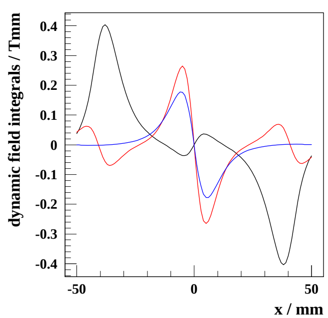

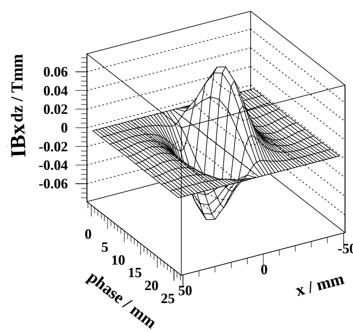

inclined mode

J. Bahrdt et al., SRI 2007

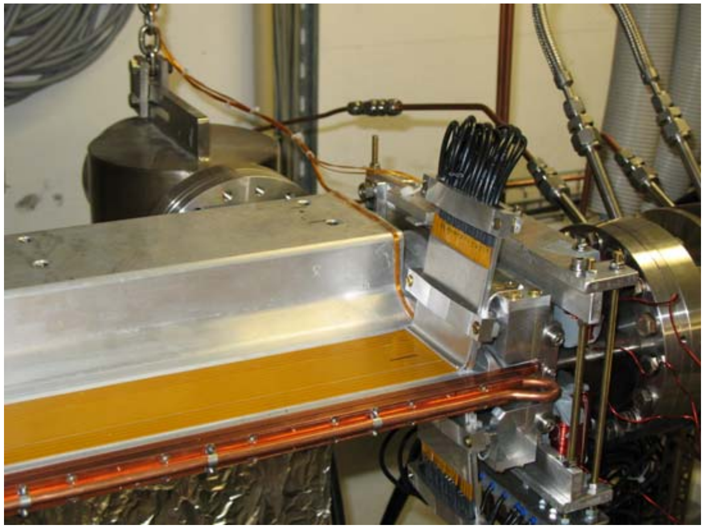

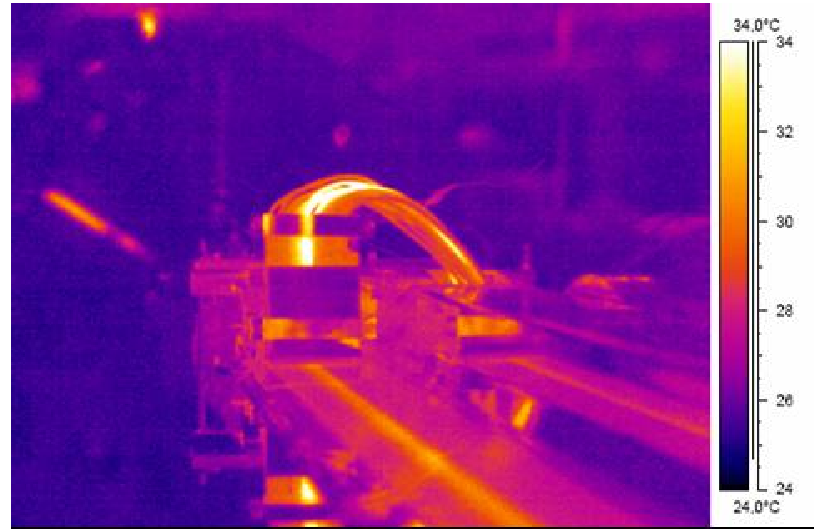

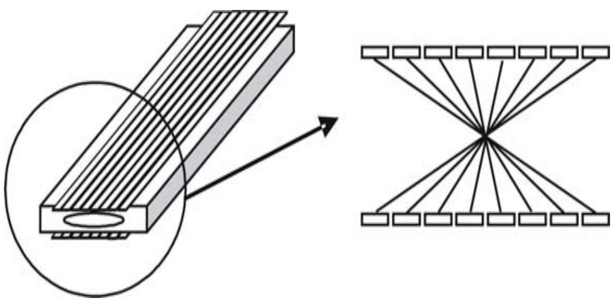

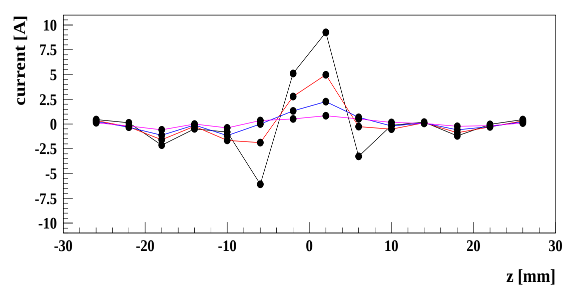

2 x 14 wires, 14 power supplies
maximum currents: 16A
wire diameter: 3 x 0.3mm**2
wire separation: 4mm

Current settings for gaps of 20mm
24mm, 30mm and 40mm

J. Bahrdt et al., EPAC 2008

UE112: Active Shimming of DM With Flat Wires II

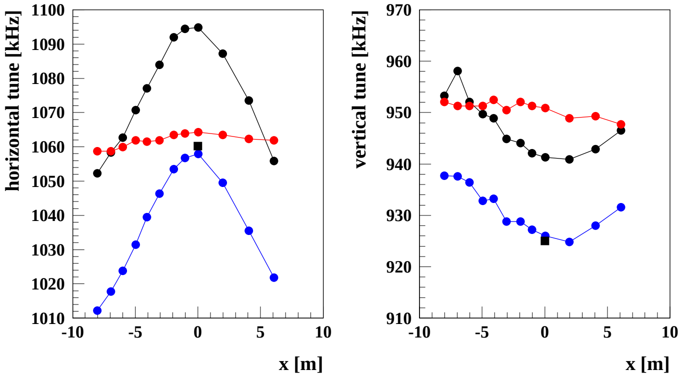

Horizontal and vertical tunes
vs horizontal displacement
black: without compensation
blue: quadrupole compensation
red: compensation with flat wires

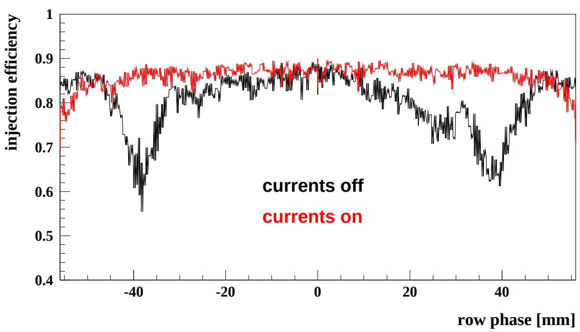

Injection efficiency with UE112
black: without compensation
red: with compensation

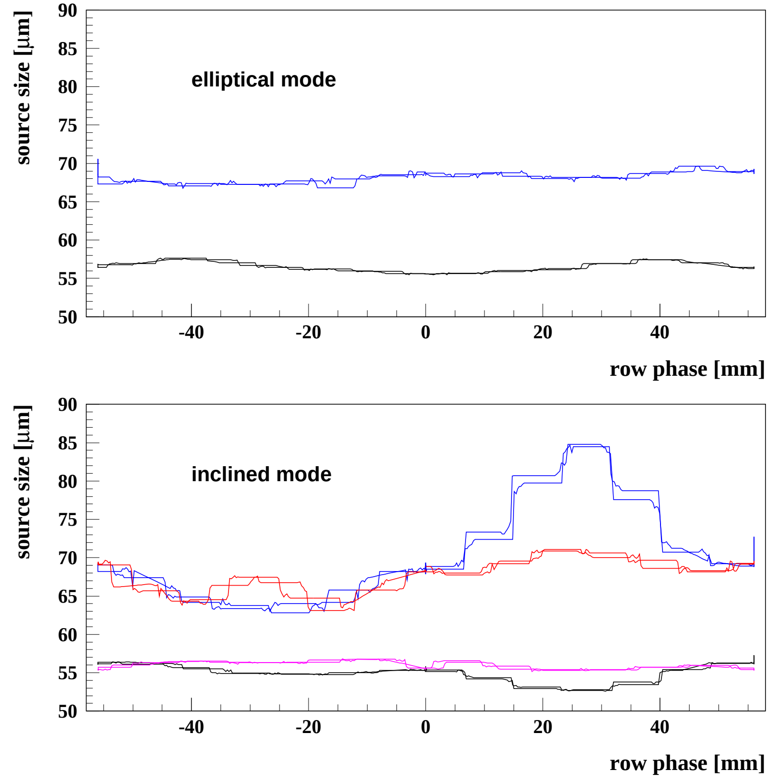

Source size variation with row phase of the UE112 at gap = 24mm in the elliptical mode (top) and the inclined mode (bottom). Black, blue: currents switched off; red, magenta: currents switched on.

Undulator fields can not be represented with 2D-multipoles due to limited radius of converence

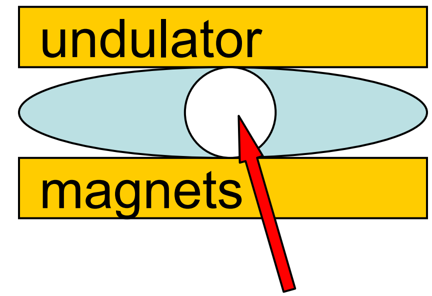

Procedure

- evaluation of transverse field distribution of one magnet row
- Fourier decomposition of these distributions
- analytical Ansatz for complete undulator structure
- similar procedure for field integrals of Fe-shims
- generate analytic expresison for scalar potentials of main field and shim field integrals
- use this scalar potential in generating function algorithm

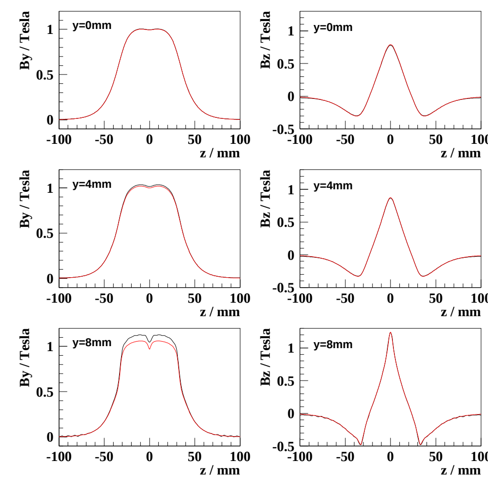

disc of convergence

accuracy of field model

Horizontal phase space

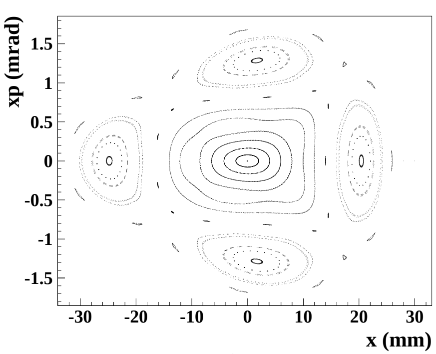

without flat wires

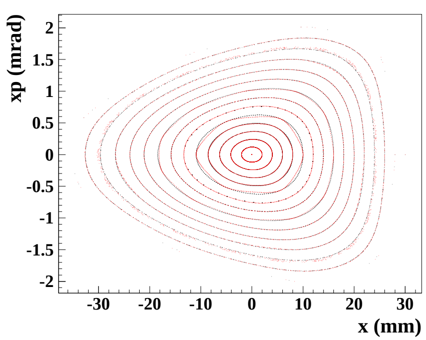

with flat wires

J. Bahrdt, M. Scheer, G. Wuestefeld, Mini-Workshop, Frascati, 2005
J. Bahrdt et al. SRI, Daegu, Korea, 2006
G. Wüstefeld, J. Bahrdt, EPAC 2006
J. Bahrdt et al., PAC 2007, EPAC 2008

HGHG-FEL at MAX-lab, Collaboration with HZB

Laser
λs = 266.66 nm
FLAT TOP shape
peak power: 300 MW
pulse duration: 300 fs fwhm

Modulator
λu = 0.048m
30 periods
λs

Radiator
λu = 0.056m
30 periods
$\lambda s/3$ - $\lambda s/5$

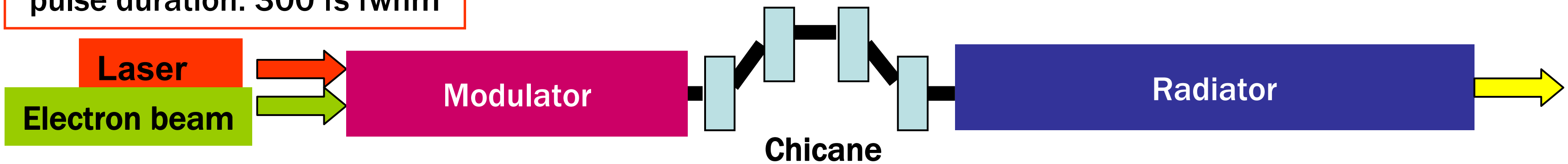

Electron beam

$\varepsilon_{nx}=\varepsilon_{ny}$= 3 mm.mrad
I_{peak}= 500 A
100μm (rms) bunch length
E_{beam} = 420 MeV
rel. e-spread = 0.1%
$\sigma_x = \sigma_y$ = 300 μm

Chicane
4x dipol magnets:
length: 0.12 m
field: ~0.15 T
separation:
distance: 0.4 m

Collaboration between MAX-lab and HZB
- test bed for studies of seeded FEL scheme
- test of specific diagnostic hardware for future light source e.g. Cherenkov, Powermeter glass fibers, THz detectors

Long Undulators for SASE-FEL Application

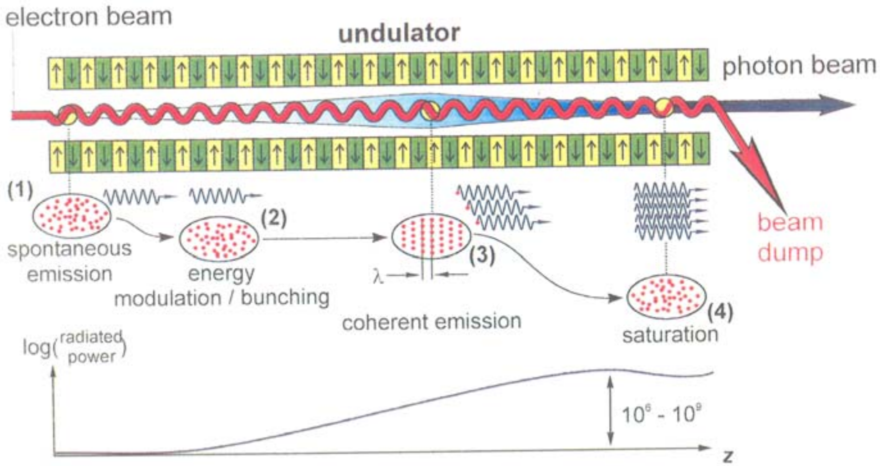

saturation demonstrated:

VISA	800 nm
LEUTL	300 nm
FLASH	6.4 nm
SPRING8 VUV	60 nm
LCLS	0.15nm

projects:

XFEL	0.1 nm
SPRING8 X-ray	0.15 nm
(SLS X-Ray FEL	0.1 nm)

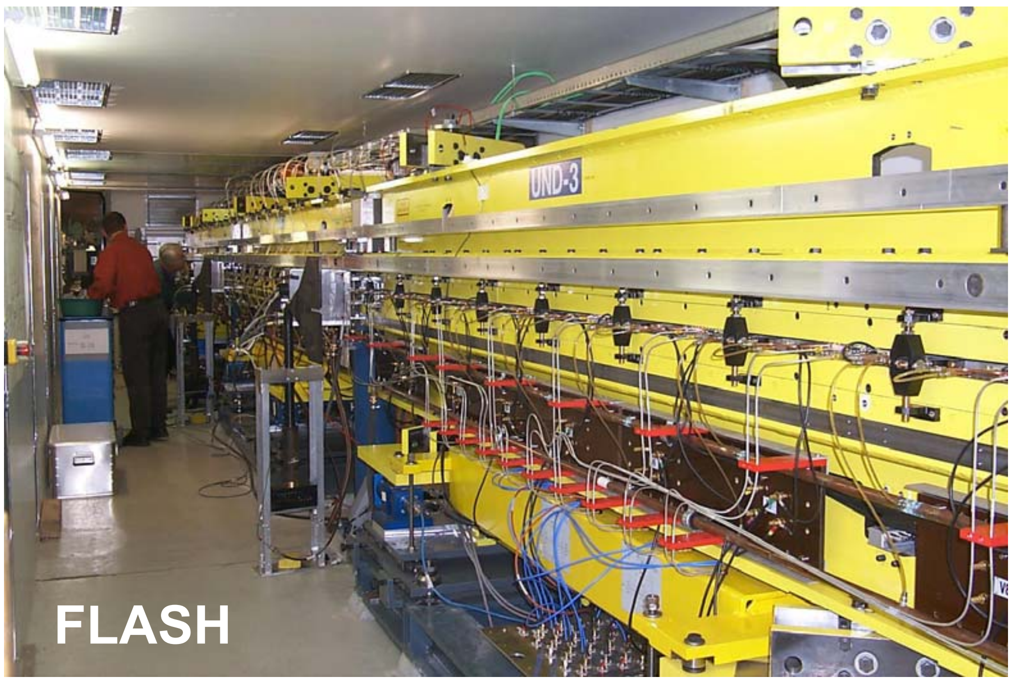

Undulator:

λ_u= 27.3 mm

Gap = 12 mm

B_{peak} = 0.46 T

K = 1.17

L ≈ 15 m

fixed gap undulators

Courtesy of J. Pflüger, XFEL

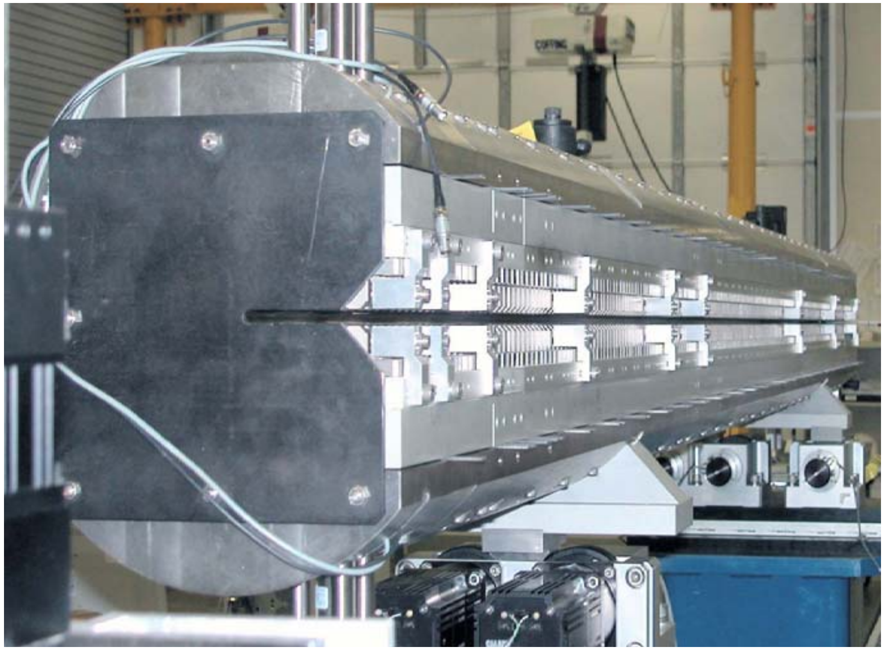

S. Milton, WUS workshop,
DESY, Hamburg, Germany, 2005

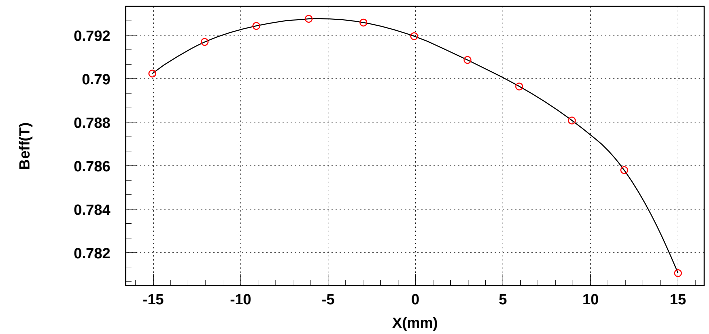

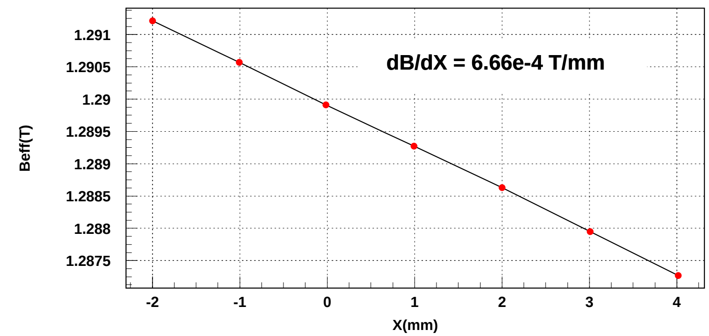

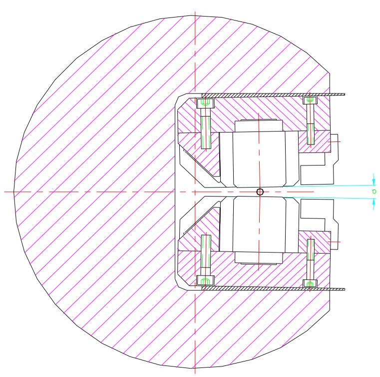

canting of poles
for fine tuning
of K-parameter

fine tuning via transverse
displacement of undulator
using cam shaft movers

fixed gap undulators

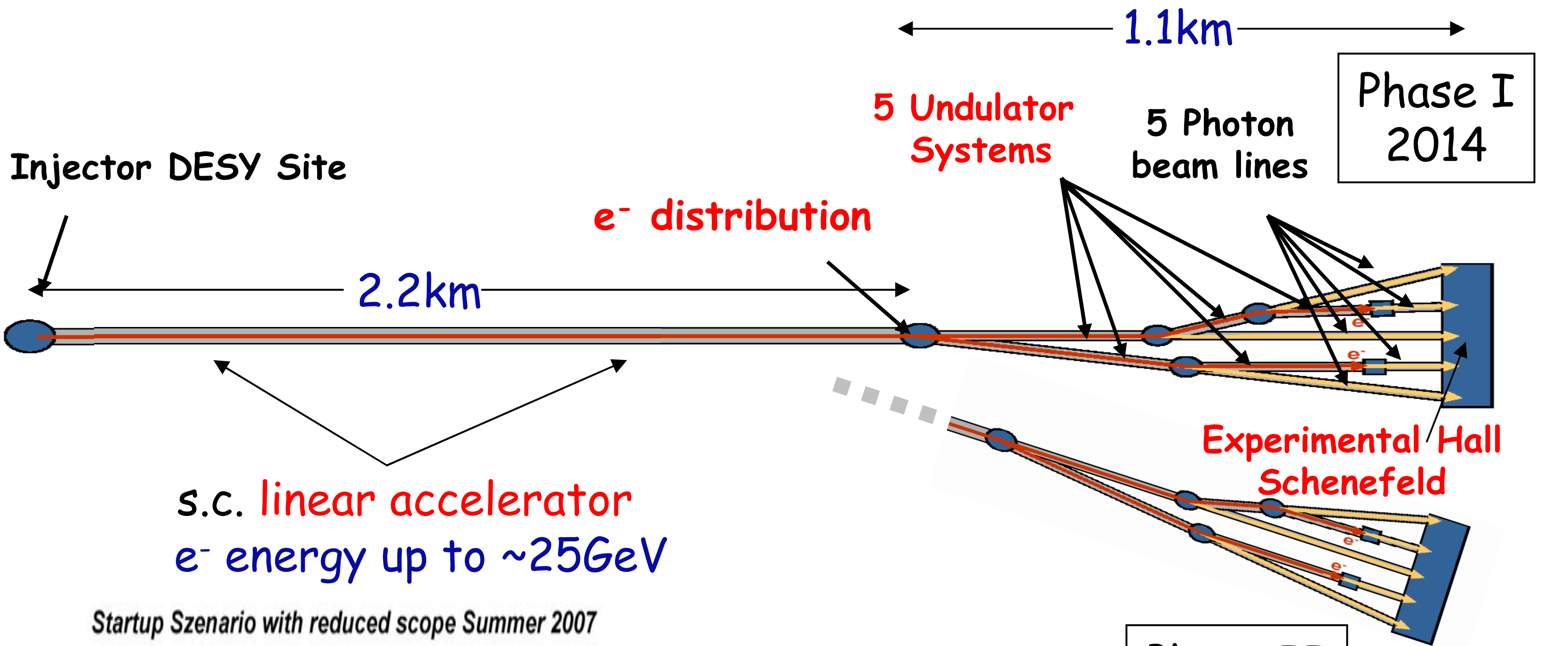

Phase II later

Courtesy of J. Pflüger, XFEL

Startup Szenario with reduced scope Summer 2007

	λ_R [Å]	λ_0 [mm]	Gap [mm]	B_0 [T]	K	β_0 [m]	L_{Sat} + [m]	N_{Tot} ++	L_{Tot} +++ [m]
SASE 1 *	1	35.6	10	1.0	3.3	32	133	33	201.3
SASE 2 *	1-4	48	19-10	0.63-1.37	2.8-6.1	46-15	174-72	37	225.7
SASE3P *	4-16	65	23-10	0.66-1.76	4.0-10.7	15	≈100	21	128.1
							Total	91	555m

* Planar Hybrid Undulator
** 1st Harmonic of Spontaneous Emitters
\+ Net saturation length with no contingency for field errors
++ Number of 5m undulator segments including 20% contingency
+++ Total system length includes 1.1m long intersection after each undulator segment

60 tons of permanent magnets